SUPPLEMENTARY TEXT (S1)

List of Abbreviations

ACC	Almora Crystalline Complex	(S.39)
AKSZ	Achankovil Shear Zone	(S.44)
AlPaCa	Alpine-Carapathian-Pannonian system	(S.23)
AMSZ	Azul Megashear Zone	(S.13)
BGB	Belleterre Greenstone Belt	(S.5)
CAOB	Central Asian Orogenic Belt	(S.47)
CCF	Castle Cove Fault	(S.55)
CCSZ	Central Cameroon Shear Zone	(S.33)
CITZ	Central Indian Tectonic Zone	(S.42)
CSZ	Chelmos Shear Zone	(S.29)
DFS	Doruneh Fault System	(S.34)
EBSD	Electron Back Scattered Diffraction	(S.24)
EGB	Eastern Ghats Belt	(S.43)
GCT	Great Counter Thrust	(S.40)
GTSZ	Gavilgarh-Tan Shear Zone	(S.42)
KMF	Khlong Marui Fault	(S.45)
LPO	Lattice Preferred Orientation	(S.20)
LSZ	Lewisian Shear Zone	(S.17)
LT	Low temperature	(S.29)
MCT_U	Main Central Thrust Upper	(S.41)
MFZ	Mitoke Fault Zone	(S.51)

MLFZ	Moonlight Fault Zone	(S.56)
MGSZ	Major Gercino Shear Zone	(S.12)
MKFB	Mary Kathleen Fold Belt	(S.54)
MLDSZ	Malpica-Lamego Ductile Shear Zone	(S.19)
MPF	Mae Ping Fault	(S.45)
MSZ	Makhbiyah Shear Zone	(S.35)
MTFZ	Møre-Trøndelag Fault Zone	(S.14)
MTL	Median Tectonic Line	(S.51)
NAFZ	North Anatolian Fault Zone	(S.30)
NATZ	North Almora Thrust Zone	(S.39)
NFC	Nevado-Filabride Complex	(S.21)
NSRD	Northern Snake Range décollement	(S.8)
PF	Pochengshan Fault	(S.47)
PSZ	Plattengneiss Shear Zone	(S.24)
RF	Rangong Fault	(S.45)
RRFZ	Red River Fault Zone	(S.46)
SBF	Southern Bounding Fault	(S.47)
SFSZ	South Finland Shear Zone	(S.16)
SGT	Southern Granulite Terrain	(S.44)
SLFZ	Sticklepath-Lustleigh Fault Zone	(S.18)
SSZ	Somero Shear Zone	(S.16)
$STDS_L$	South Tibetan Detachment System-Lower	(S.37)
$STDS_U$	South Tibetan Detachment System-Upper	(S.37)
STTFZ	Southern Troodos Transform Fault Zone	(S.31)

TMC	Tso Morari Crystallines	(S.38)
TPF	Three Pagodas Fault	(S.45)
TSZ	Teslin Suture Zone	(S.3)
UHT	Ultra-high temperature	(S.22)
VSSZ	Vals-Scaradra Shear Zone	(S.25)
XF	Xinxingxia Fault	(S.47)
YFZ	Yamasaki Fault Zone	(S.51)
YRSK	Yukon River Shear Zone	(S.2)
ZSZ	Zanskar Shear Zone	(S.37)

S. Reports of OSS from across the globe (Fig. 24)

OSS has been identified from different terranes worldwide (**Table II; Fig. 24**). We compile as many examples as we could, however, the list may not contain all the examples. A few examples of conflicting shear senses with non-parallel shear planes have been included. Below, we briefly describe each of the terranes. The locations are arranged continent-wise i.e. N. America (1 to 8) → S. America (9 - 13) → Europe (14- 31) → Africa (32 and 33) → Asia (34-51) → Australia (52-55) → Zealandia (Mortimer et al., 2017, 2018) (56) **(Fig. 24)**.

S.1 Franklinian Basin, Ellesmere Island, Canada

De Paor & Eisenstadt (1987) utilize the theory of 'null points' (Section 4.2.1; **Fig. 17**) to infer a single episode of reversal across a (sub-)vertical fault during Ordovician times in the Franklinian Basin (Canada). However, they do not state any reason for reversal in particular for this.

S.2 Yukon River Shear Zone (YRSK), Canada

The ~ NW-SE striking YRSZ crops out within and cuts across the Yukon-Tanana terrane in the central belt of the North American Cordillera. The YRSZ separates the Early Carboniferous orthogneisses to the north from the Mid-Permian plutonic rocks to the south (Ryan et al., 2014). Parsons et al., (2018), based on U-Pb zircon dating of orthogneisses, show that the region deformed four times between ~ 259 to < 176 Ma. The authors further state that the YRSZ records ductile top-to-ESE shear, as identified in both meso-scale (e.g., asymmetric sigmoid K-feldspar augens and asymmetric boudins) and micro-scale (e.g., quartz shape preferred orientation, quartz CPO fabrics), during ~ 259–176 Ma at amphibolite-eclogite grade conditions. It reactivated with a top-to-WNW sense post-176 Ma

(Ar-Ar date on muscovites; Joyce et al., 2015), as a brittle thrust producing fault propagation folds.

S.3 Teslin Suture Zone, Canada

The ~ 200 km long, ~ 10 – 15 km thick and ~ NW-SE trending ductile shear zone marks the southern extent of the Yukon-Tanana terrane in Canadian Cordillera. The shear zone can be traced from Alaska (USA) to British Columbia (Canada) for > 1000 km (Hansen, 1989). The Teslin Suture Zone (TSZ), also referred to as the Teslin tectonic zone, consists of intensely deformed greenschist-amphibolite grade metasediments (L-S tectonites) locally intruded by Late Triassic-Early Jurassic plutons (Hansen & Dusel-Bacon, 1998). It separates the allochthonous Late Paleozoic-Early Mesozoic oceanic terrane from the parachthonous Proterozoic-Paleozoic rocks of the North American Cordillera that lie to the west and east of the TSZ, respectively (Tempelman-Kluit, 1979). The TSZ is bound by thrust and strike-slip faults on the eastern and western sides, respectively (Dusel-Bacon et al., 1995). Hansen (1989, 1992) report the presence of ductile shear sense indicators viz., S-C fabrics, quartz pressure shadows, small-scale folds, from the tectonites indicating normal, reverse and strike-slip shear. The author interprets them to represent W-dipping subduction channel-related pre-195 Ma deformation features, where the sequence of deformation has been top-to-E (up) (subduction / downflow) followed by dextral strike-slip and top-to-W (down) (exhumation / backflow).

S.4 Ruby Mountains, USA

The ~ 60 km long and ~ 20 km wide ~ NE trending Ruby Mountains are a part of the North American Cordillera and are exposed near the northwestern Wyoming. The major rock types are igneous and metasedimentary mylonitic granites and gneisses (Colgan et al., 2010). These lithounits exhibit both the top-to-S (up) and top-to-N (down) shear, with the latter possibly developed in response to the gravity or thermal weakening-induced topographic collapse of the thickened crust (Sousa, 2008).

S.5 Belleterre Greenstone Belt (BGB), Canada

The BGB is the youngest greenstone belt in the Archean Canadian Shield. Often described as a thrust sheet, it is dominantly composed of volcanics and metasediments (Sawyer & Barnes, 1994). The BGB is also known for its rich deposits of Ni-Cu sulfides (Barnes et al., 1993).

Structural complexity of the area has arisen due to reversal in shear senses. Based on the asymmetry of folds, shear bands and the orientation of three sets of veins (V1: ~ NW-SE, V2: ~ E-W, and V3: ~ NNE-SSW trending) on horizontal outcrop, Tourigny & Schwerdner (1991) infer that the region reversed shear sense from right-lateral to left-lateral due to separate episodes of coaxial deformations as the principal compressive stress axes reoriented from NW-SE to NE-SW.

S.6 Portuguese Bend landslide complex, USA

This 30 – 50 m thick complex lies ~ 30 km to the south of Los Angeles (USA) and covers ~ 6 km^2. The active slide area is deformed internally and has moved seaward, towards west, at ~ 3.3–3.8 mm yr^{-1} in between the years 1956 and 2002 (Kayen et al., 2002; Calabro et al., 2010). Based on the arrangement of lithounits across a NNE-SSW trending strike-slip fault, Larue & Hudleston (1987) report both sinistral and dextral slips. The authors further state that the latter shear is a late-stage reactivation. However, they do not provide a suitable tectonic model for this.

S.7 Pinal Peak, USA

The Paleoproterozoic Pinal Schist is dominantly composed of lower greenschist facies rocks, quartzite and volcanics, and constitutes an~ E-W trending > 5 km thick shear zone from the Pinal mountains of SE Arizona (Keep, 1996). Based on S-C fabrics, microfolds, mica fish (ten Grotenhuis et al., 2003), quartz c-axis fabrics etc., Hansen & Keep (1994) identify both top-to-S (up) and top-to-N (down) shears from within the Pinal Schist, with the former sense being dominant. The authors also report a mismatch between the shear sense obtained from the quartz c-axis fabrics and other microstructures (listed above) from the same rock samples. However, they do not provide a conclusive reason.

S.8 Northern Snake Range Mylonite Zone, USA

This ~ N-S trending and ~ 30 km long mylonite zone is a part the Cordilleran metamorphic complex and crops out in the eastern Nevada (USA). It constitutes the footwall rocks of the Northern Snake Range décollement (NSRD). These rocks (mostly schists and quartzites) deformed twice since the Late Cretaceous to Tertiary, and both coaxial and non-coaxial shear presumably affected them (Lee et al., 1987). Cooper et al. (2010) report both top-to-E (shear bands and asymmetric porphyroclasts) and top-to-W (mica fish, shear bands and calcite SPO) shear senses from the mylonites, with the latter overprinting the former **(Fig. S3a** in the supplementary file **S2)**. The authors propose that the mylonites reversed shear during exhumation as they passed over the upper hinge of a '*rolling hinge system*' (Axen et al., 1995).

{Insert Fig. S2 about here}

S.9 Itacaiúnas Belt, Brazil

This E-W trending belt is dominantly composed of high grade gneisses and medium grade (amphibolite facies) orthogneisses (2.85 Ga, U-Pb zircon dates from gneisses and migmatites of Xingu Complex by Machado et al., 1991). It lies to the south of the Amazon Basin of the Amazonian Craton, and consists of two major E-W trending Archean (~2.6 Ga) strike-slip systems viz., Carajás and Cinzento fault zones. Together, these sigmoid anastomosing discontinuous network of strike-slip faults, presumably step-overs or over-steps (e.g., Mukherjee 2013b), occupy ~ 200 km long and ~ 80 km wide zone (Holdsworth & Pinheiro, 2000). Pinheiro & Holdsworth (1997) report that the stress regime in the region oscillated between NE-SW compression (sinistral transpression) and NE-SW extension (dextral transpression), and therefore the strike-slip system underwent slip reversals thrice between 2.8 and 1.0 Ga.

S.10 Senador Pompeu shear zone and Bação complex, Brazil

Hippertt & Tohver (1999) report opposing shear within each of the mylonitic samples collected from the Senador Pompeu shear zone and the Bação complex in NE and the SE Brazil, respectively. The authors discuss that progressive deformation under general shear conditions can induce rheological changes within different domains of the same rocks with passage of time. Under such circumstances, the shear senses at the domain boundaries may be opposite to that of the overall deformation.

S.11 Quadrilátero Ferrífero, Brazil

This granite-greenstone terrane of the Brazilian Precambrian shield has undergone two major tectonic events viz., the Transamazonian extension followed by a compressional Brasiliano orogeny (~ 0.8 – 0.6 Ga, U-Pb geochronology of zircons from granitic intrusions by Chemale et al., 2012). Hippertt & Davis (2000) report OSS within ~ 10 m from the Moeda Syncline.

The mylonites at the contact between the limbs and the surrounding granite-gneiss domes show a ductile shear sense opposite to that preserved in the bedding parallel shear zones within each limbs. This conflict has possibly arisen as a result of separate processes viz., folding (interlayer shear zones) and exhumation of domes (contact shear zones) during the Brasiliano compressional deformation event.

S.12 Major Gercino Shear Zone (MGSZ), Brazil

The ~NE-SW striking MGSZ lies within the Santa Catarina Shield (S Brazil), and demarcates the metavolcanic sediments from the Florianópolis Batholith that lie to the SE and NW, respectively (Chemale et al., 2012; Hueck et al., 2018). MGSZ forms a part of ~ 1000 km long Dom Feliciano Belt (Neoproterozoic to Early Paleozoic), and is exposed for ~ 70 km near the city Florianópolis. This shear zone is ~ 10 km wide but thins to a few km at NE. The major rock type is granitic mylonite, with sporadic phyllonites that dominantly bear shear sense indicators viz., S-C fabrics and asymmetric K-feldspar porphyroclasts indicating a dextral transpression. U-Pb zircons dates from the shear zone bracket the age of onset of dextral transpression between 615 to 609 Ma (Passarelli et al. 2010). However, Hueck et al. (in press), report symmetric θ and φ clasts from thin-sections along with mica fish, oblique foliations and Quartz CPO fabrics exhibiting sinistral deformation. The authors further observe stretching lineations parallel to the axes of the intrafolial folds, and propose this OSS to be a consequence of pure shear-dominated deformation in the MGSZ.

S.13 Azul megashear zone, Argentina

The ~ E-W trending ~ 40 km long Azul Megashear Zone (AMSZ) consists of proto- to ultramylonitized granites exposed in the Rio de la Plata craton. The AMSZ exhibits both sinistral and dextral slip, deciphered from shear bands and asymmetric mantled porphyroclasts etc. at outcrop scale. Thin-section observations too reveal OSS both top-to-N and top-to-S ductile shear senses based on σ and δ-porphyroclasts, S-C fabric, biotite fish etc. (Frisicale et al., 2005). The reason of this OSS has remained unexplained.

S.14 Møre-Trøndelag Fault Zone (MTFZ), Central Norway

The ENE-WSW to NE-SW trending MTFZ is a prominent regional feature that crops out in central Norway and continues for > 300 km from onshore to offshore (Redfield et al., 2005). The onshore portion of the fault zone is primarily composed of gneisses, metagranotoids, amphibolites, and low grade- greenschist facies and/or lower- metasediments. In the offshore, MTFZ separates the Møre Basin and the Viking Graben that lie to its north and south, respectively. The MTFZ has a complex tectonic history that involves multiple reactivations: both dextral and sinistral strike-slip as well as vertical motions (Grønlie & Roberts, 1989; Serrane, 1992; Redfield et al., 2004). Field studies by Serrane (1992) reveal shear sense switch from top-to-NE (~ 400 Ma, Rb-Sr whole rock dating of granites by Tucker & Kogh, 1988) to top-to-SW (~ 390 Ma, Ar-Ar dating of the muscovites in the shear zone mylonites by Chauvet & Dallmeyer, 1982) by post-orogenic extensional collapse.

S.15 Bergen Arc Shear Zone, Norway

Continental collision between Baltica and Laurentia, the Caledonian Orogeny, took place during ~ 440 - 420 Ma. The Bergen Arc is a high metamorphic belt that lies within this collisional terrane and exposed in SW Norway (Putnis et al., 2017 and references therein).

Wennberg (1996) discusses that the structural complexity of the Bergen Arc Shear Zone that comprises of both top-to-NW and top-to-SE ductile shear indicated by asymmetric pinch and swell structures, shear bands, folds etc. The author propose that this complicacy has arisen due to the overprinting of the later top-to-NW deformation (post-orogenic extension) on to an earlier top-to-SE shear due to collision-induced thrusting. Harris et al. (2002) also report similar overprinting of deformation fabrics from the Caledonides in the southern Norway.

S.16 Svecofennian Shear Zones, Finland

The Somero and South Finland Shear Zones (SSZ and SFSZ, respectively) trend ~ E-W and extend for ~ 200 km in SW Finland. The two shear zones originated during the Svecofennian orogeny (~ 1.8 Ga, U-Pb dating of titanites and zircons in mylonitic gneisses by Torvela et al., 2008), and are connected by several steep ~ N-S trending faults. The dominant rock types are granites, tonalitic gneisses and pseudotachylites (Torvela et al., 2008). Field studies reveal brittle reactivation of the SSZ and SFSZ resulted in reversal of the slip sense from dextral to sinistral. This shear reversal occurred in response to the late ~ E-W extension (Väisänen & Skyttä, 2007).

S.17 Lewisian Shear Zone (LSZ), Scotland

The LSZ, a narrow (< 100 m wide) NW-SE trending zone of mylonitised gneisses, is a part of the larger Archean-Proterozoic Lewisian complex composed mainly of high grade quartzo-feldspathic gneiss exposed in NW Scotland (Park et al., 1987). The rocks deformed at least four times between ~ 2.6 – 1.4 Ga (review in Wheeler et al., 2010). Field-based kinematic studies reveal a series of shear reversals in the LSZ. Ductile mylonites showing left-lateral shear (asymmetric boudins, S-C fabrics etc.) are cross-cut by brittle right-lateral shear (R and R' shear). Lei & Park (1993) propose a change in regional compression from NW-SE to N-S for the same. This was followed by another reversal to brittle left-lateral shear due to the clockwise rotation of the area relative to a nearby regional dextral strike-slip Flowerdale fault system.

S.18 Sticklepath-Lustleigh fault zone (SLFZ), UK

The SLFZ is a WNW-ESE trending and ~ 65 km long strike-slip fault that originated along with several other strike-slip faults during the Varisican Orogeny (Holloway & Chadwick, 1986 and references therein) due to oblique collision between the Gondwana and the Baltica-Laurentia (Matte, 2001).

Holloway & Chadwick (1986) discuss two episodes of shear reversals along the SLFZ. The initial right-lateral offset of the Permian rocks across the SLFZ was followed by ~ 6 km left-lateral displacement along SLFZ during Early Tertiary due to extension in SW England creating pull-apart basins viz. Bovey, and Petrockstow. Local dextral movements occurred along the SLFZ during the Mid-Tertiary.

S.19 Malpica-Lamego Ductile Shear Zone (MLDSZ), Spain

The ~ 275 km long MLDSZ crops out in the NW part of the Iberian Peninsula, from Malpica (Spain) in the north to Penedono (Portugal) to the south, as an arcurate structure with ~ NW-SE trend paralleling theVariscan belt (Llana-Fúnez & Marcos, 2001). The rock types of the MLDSZ are dominantly mylonitic schists, granites and gneisses with sporadic metasediments. These rocks underwent four phases of deformation under amphibolite to greenschist facies conditions (Dias & Ribeiro, 1995). The northern segment of the MLDSZ is deformed more complexly and records slip reversal from dextral to sinistral (Llana-Fúnez & Marcos, 2007 and references therein). Pamplona et al. (2016) report sinistral strike-slip near the central segment of the MLDSZ and relate to the intracontinental reactivation tectonics of the Variscides.

S.20 Ronda peridotite, Spain

This ~ 5 km thick and southerly dipping tectonic unit, exposed in SW Spain, is the largest orogenic peridotite covering > 450 km^2. It crops out in the hinterland of the arcurate Betic Cordillera orogen, which formed due to the collision of Iberia and Africa in the Early Miocene. It is an intensely foliated SW-NE trending body of mylonitic garnet-bearing peridotites. Besides, this ultramafic rock massif also consists of lherzolites, harzburgites, dunites and foliation parallel layers of pyroxenites (Platt et al., 2003, 2013). van der Wal & Vissers (1996), through olivine LPO fabrics, identify two shear zones within the peridotite body with opposing ductile shear senses viz. top-to-N followed by top-to-S. The temporal relationship was established based on the *(i)* petrological/mineralogical study involving identification of the metamorphic facies, and *(ii)* structural observations viz., deformation heterogeneity/strain localization.

S.21 Nevado-Filabride Complex, Spain

The Nevado-Filabride Complex (NFC) constitutes a part of the Alboran domain, which collided with the southern (paleo-) margin of the Iberia producing the Betic Cordillera (Puga et al., 2017). However, Platt et al. (2006) propose that the NFC is rather a part of the Iberian paleomargin itself, and characterizes subduction-related HP metamorphism. Exposed as E-W trending antiformal core complex, the NFC is present only in the eastern and central parts of the Betics. The major rock types in the NFC are Paleozoic dark schists, mylonites, cataclasites, and Triassic marbles (Weijermars, 1991 and references therein; Augier et al., 2005). It deformed at least four times from Late Cretaceous to Mid-Miocene (Aerden et al., 2013; Platt et al., 2013 and references therein). Ruiz-Fuentes & Aerden (2018) report OSS, top-to-W and top-to-E, from the shear bands present in a single outcrop of schistose rocks of the NFC. In both the cases, the S_4 and S_2 define the S- and C-plane, respectively. However, Ruiz-Fuentes & Aerden (2018) did not explain the reverse shear.

S.22 Bohemian Massif, Central Europe

Paleozoic collision between the Gondwana and the Laurussia developed the Variscan fold thrust belt (Fernández et al., 2016 and references therein). This 'fossil' orogen preserves signatures of both Andean- and Alpine-type collisions. The Bohemian Massif lies at the eastern end of the Variscan fold thrust belt, and hosts several UHT and UHP rocks (Schulmann et al., 2014 and references therein).

Several NW trending strike-slip faults within the Bohemian Massif, viz. Pfahl, Danube, Franconian and the Intra-Sudetic, underwent reversed slip from dextral (~ 380 Ma) to sinistral (~ 290 Ma) (Mattern, 2001 & references therein), possibly due to the orthogonal switch (~ N-S → E-W) of the compression direction coupled with the changing positions of the Baltica and Western Europe since Late Paleozoic (Torsvik et al., 1996) Uralian orogeny. However, Galadí-Enríquez et al. (2006), based on the oblique shape preferred orientation of the quartz grains, report late shear reversal from sinistral to dextral.

S.23 Alpine-Carpathian-Pannonian region, Austria

The Alpine-Carapathian-Pannonian system (AlCaPa) lies within the NW part of the Pannonian Basin (Central Europe) originated during the collision between the European and the Adriatic plates (~ 55–17 Ma) (review in Carminati & Doglioni, 2012). The N-S compression produced NNW-directed thrusting and was followed by an E-W compression (Beidinger & Decker, 2016). This late-stage reorientation of the stress regime caused brittle reactivation and reversed slip sense along NW-SE and NE-SW trending dextral (~ 10 km long Feichtbauer and Trattenbach faults, ~ 40 km long Wolfgangsee and Windischgarsten faults) and sinistral (Salzachtal-Ennstal fault, ~ 300 km) strike-slip faults, respectively (Peresson & Decker, 1997).

S.24 Greiner shear zone and Koralpe range, Eastern Alps, Austria

The ~ ENE-WSW trending > 35 km long Greiner shear zone exposed within the Tauern Window, which is bounded by extensional faults and exposes the deepest litho-units of the European basement in the form of upright folds (Rosenberg et al., 2018), of the eastern Alps. The shear sense in dominantly sinistral, however, dextral motion has also been reported from the same. Barnes et al. (2004) propose that the localized occurrences of the dextral shear relates to the devolatilization of the metaserpentinites. The fluid released created weak zones within the granodiorites along which the late stage (post 26 Ma, in situ dating of monazite grains) dextral deformation localized. The ~ WNW-ESE trending Periadriatic Lineament south of the Tauern Window also recorded a shear reversal from sinistral to dextral at ~ 30 Ma (Rb-Sr dating of muscovites by Mancktelow et al., 2001; Pleuger et al., 2012). Detailed field-based structural studies carried out in the same region by Ceccato & Pennacchioni (2018) reveal a localized switch in shortening direction from ~ E-W to ~ N-S in Late Oligocene.

The Koralpe range (~ NW-SE trending) is ~ 40 km SW of the city Graz (Austria) and consists of metapelitic and metapsammitic rocks. Hatley et al. (2009), based on EBSD studies of the mylonites of the Plattengneiss Shear Zone (PSZ) located at the southern part of the Koralpe range, identify an up-section transition from top-to-S to top-to-N shear near the central portion of the PSZ.

S.25 Vals-Scaradra Shear Zone (VSSZ), Switzerland

The ~ WSW-ENE trending VSSZ, which was active ~ 35–30 Ma (Löw, 1987), marks the northern end of the HP eclogite facies rocks of the Adula Nappe, Central Alps. Based on asymmetric porphyroclasts, mica fish, shear bands and quartz c-axis fabrics, Kossak-Glowczewski et al. (2017) report an along-strike variation in slip sense of the VSSZ. The western part of the VSSZ sheared sinistrally (top-to-W), however, in the eastern part it is opposite. The authors propose that the VSSZ inhibited the northward propagation of the Adula Nappe, and thereby assisted to its lateral motion in opposite directions. The reverse shear senses are attributed to this lateral spreading. The authors also compare the origin of the VSSZ to that of stretching faults (Means, 1989, 1990) (Section 4.1, **Fig. 15**), wherein along-strike shear reversals result from stretching or shortening parallel to the fault itself.

S.26 Combin & Zermatt-Saas zones, Italy

These zones are located in the Swiss-Italian western Alps. The Zermatt-Saas zone (eclogite-facies) consists of the UHP Lago di Cignana unit, and is separated from the overlying Combin Zone (greenschist to blueschist-facies) by the northerly dipping Combin Fault. The (U)HP Zermatt-Saas zone rocks at the upper structural levels underwent syn-exhumational (~ 38 Ma, whole rock Rb-Sr dating by Amato et al., 1999) top-to-SE (down) ductile shear. This was later (~ 35 Ma, based on the Ar-Ar and Rb-Sr geochronometry by Reddy et al., 2003) overprinted by post-exhumational, semi-ductile top-to-NW shear (sub-horizontal shear plane), which resulted in response to a phase of pure shear (Kirst & Leiss, 2017 & references therein). The late stage coaxial deformation under greenschist facies produced conjugate top-to-NW and top-to-SE shears.

S.27 Alpine Corsica, Corsica Islands, France

The Alpine Corsica orogenic wedge represents a nappe stack of tectonic units derived both from continental and oceanic crusts that formed during the Alpine orogenesis (~ 30 Ma back) (Jolivet et al., 1991; Rossetti et al., 2015; Beaudoin et al., 2017). It underwent two major tectonic events viz., *(i)* Late Cretaceous–Mid Eocene collision and crustal thickening, and *(ii)* Early Oligocene-Mid Miocene extension and rifting (Jolivet et al., 1990, 1991; Turco et al., 2012). This late-stage extension of the thick crust overprinted top-to-E (down) shear over a prior top-to-W (up) shear along the reactivated thrust contacts, and reorientation of the quartz CPO fabrics. Shear bands, formed at greenschist facies condition, show a top-to-W shear. These bands cross-cut east dipping foliations defined by high P-low T minerals (amphiboles) (Jolivet et al., 1990 and references therein).

Beaudoin et al. (2017) also report a slip reversal in the Alpine Corsica, Tenda massif in particular. The authors identify syn-burial top-to-SW ductile shear structures overprinted by late stage syn- exhumational top-to-NE shear, both at outcrop-scale and in thin-sections. The intensity of this later deformation decreases towards the core of the massif.

S.28 The Apennines, Italy

The arc-shaped and NE-verging Apennines fold-thrust belt developed by collision between the European (Corsica-Sardinia block) and the Adrian plates during the Alpine Orogeny (Carmignani & Kligfield, 1990; Doglioni et al., 2007; Carminati & Doglioni, 2012). Evidences of both pre- and post-orogenic extension are preserved in this orogenic belt (Butler et al., 2006; Decarlis et al., 2013). Tectonic/structural inversion (Section 4.2.1) i.e., reactivation of a normal or reverse fault with an opposite slip sense have been reported by several authors viz., Tavarnelli (1999), Scisciani et al. (2002), Bigi (2006) from the Apennine fold-thrust belt. These authors have identified two episodes of extension, pre- and post-orogenic, separated by contraction. This means that both positive (Mio-Pliocene) and negative (Plio-Pleistocene) inversions (**Fig. 16**) have taken place. Consequently, ductile and brittle shear fabrics/structures such as S-C fabrics, sigmoid veins, crenulations, folded shear bands, and riedel shears etc., indicate either of these sequences of shear: top-to-WSW (down) → top-to-ENE (up) → top-to-WSW (down) (Tavarnelli, 1999); top-to-E (up) → top-to-W (down) (Scisciani et al., 2002); top-to-NE (up) → top-to-SW (down) (Bigi, 2006). These shears have been identified at the outcrops as well as from the thin-sections.

S.29 Chelmos Shear Zone (CSZ), Greece

The ~ 1 km thick CSZ lies within the External Hellenides, an Alpine-type orogeny. The CSZ hosts dominantly HP/LT rocks such as phyliites and quartzites (Xypolias & Koukouvelas, 2001). Xypolias & Koukouvelas (2001) report both top-to-W/SW (quartz CPO fabrics) and top-to-E/NE (S-C fabrics and asymmetric folds) from this region, however, explanation of reverse shear remains due.

S.30 North Anatolian fault zone, Turkey

The ~1300 km long North Anatolian Fault Zone (NAFZ) exhibits a curvilinear trend that varies from ~WNW-ESE near Erzincan (Turkey) in the east to ~ ENE-WSW at its western end near the Aegean Sea. It marks the boundary between the Anatolian plate to the south and the Eurasian plate to the north. The dextral-slip along the NAFZ is an artefact of the westward escape of the Anatolian plate due to its collision with the northeasterly moving Arabian plate ~11 Ma ago (Barka, 1992; Licciardi et al., 2018 and references therein). Ar-Ar dating of the volcanic rocks, offset by the NAFZ, reveal a sudden increase in the slip rate from 3 mm yr^{-1} to 20 mm yr^{-1} ~ 2.5 Ma ago (Hubert-Ferrari et al., 2009).

Hancock & Barka (1981) report two sets of mesofractures from the sedimentary basins between Erbaa and Cerkes (Turkey). One set of mesofractures (~ 5-3 Ma) demonstrates sinistral slip, whereas the other shows a dextral movement. According to the authors, the older left-lateral shear might be related to either a regional or a local stress configuration of ~ NW-SE directed extension.

S.31 Southern Troodos transform fault zone (STTFZ), Cyprus

This E-W trending, ~ 5 km thick fault zone lies to the north of the Trodos massif and marks the southern extent of the Trodos ophiolite. The fault zone mainly comprises of volcaniclastic sediments, gabbros, sheared/mylonitised serpentinites. The STTFZ cuts across the N-S trending sheeted dyke complex of the ophiolitic sequence (MacLeod & Murton, 1993; Borradaile, 2001). The contrasting nature of the volcanic rocks compared to those in the vicinity led Moores & Vine (1971) to recognize it as a fossil oceanic transform zone. Both sinistral and dextral shears are reported, with few authors suggest a reversal of slip (Dilek et al., 1990; Grand et al., 1993).

Based on faulted clasts, sigmoid shear fabrics and curved dykes at the margin of the STTFZ, MacLeoad & Murton (1993, 1995) report both sinistral and dextral shears. The latter is dominant throughout the zone, whereas the former are found in the thin mylonitised shear zones. They refute any possibility of shear reversal, and proposed that the conflicting shears may have arisen due to slip along the boundaries of rotating rigid blocks within the shear zone (**Fig. 13**).

S.32 Wadi Kid, Egypt

The Wadi Kid area, lies within the Sinai Peninsula in NW Egypt. Rifting along the Red Sea has a major effect on the structural geology and tectonics of the region, which deformed twice viz. pre-620 Ma collision and post-620 Ma extension (Fowler et al., 2010). Based on ductile kinematic indicators viz. asymmetric pressure shadows, crenulation cleavages etc., Blasband et al. (1997) report closely-spaced top-to-NW and top-to-SE shear throughout the Wadi Kid area. The authors conclude that at ~ 560-530 Ma (K-Ar dating of biotites from the younger granites, Bielski et al., 1982) the top-to-SE shear overprinted on the older top-to-NW due to intrusion-induced uplift/upwarping.

S.33 Central Cameroon Shear Zone (CCSZ), Cameroon

The ~ ENE trending CCSZ belongs to the Adamawa (also spelled as Adamaoua)-Yadé domain of the Pan-African fold belt, and comprises mainly of mylonitised migmatites, gneisses and granites (~630 – 550 Ma, based on U-Pb and Sm-Nd data of Toteu et al., 2001). The crustal structure and tectonic evolution of the CCSZ rocks resemble with those present in the Borborema Province, NE Brazil, and speculated as portions of once continuous Pan-African Brasiliano tectonic belt (~ 600 Ma) (Toteu et al., 2004; Ngako et al., 2008). CCSZ was dominantly transpressive but record both sinistral (small-scale asymmetric folds and SPO of feldspar phenocrysts) and dextral shear (shear bands and asymmetric boudins). Utilizing kinematic indicators viz. S-C fabrics, tension gashes, asymmetric folds and boudins, and obliquity of the feldspar phenocrysts, in both meso- and micro-scale, Ngako et al. (2003) propose that the CCSZ originated as a sinistral strike-slip fault, and reverse sheared during the Pan-African orogeny ~ 600 Ma.

S.34 Doruneh Fault System, Iran

This 900 km long, left-lateral strike-slip fault system lies in the Iranian segment of the Alpine-Himalayan orogen. The trend of the Doruneh Fault System (DFS) varies along its length from ~ E-W to the east (north of Afghanistan) to ~ NE-SW in central Iran, and so does its nature i.e. the DFS behaves as a sinistral transpressive system in the east, whereas to west the displacement is purely sinistral (Javadi et al., 2013; Walpersdorf et al., 2014). The sinistral slip rate at the central portion of the DFS ranges ~ 2 – 3 mm yr^{-1} (Walker & Fattahi, 2011). Based on various shear sense indicators viz. S-C fabric, tension gashes, mineral fibers, sigmoidal fractures etc., Javadi et al. (2015) report that the western portion of the DFS reversed slip sense from dextral to sinsitral at ~ 8 -10 Ma, possibly due to clockwise rotation of the maximum compressive stress axes (σ_1) from ~ NW-SE to ~ NE-SW trend.

S.35 Hilti and Wadi Tayin massifs, Oman

The 25 km long and 15 km wide Hilti massif mostly consists of peridotites and oceanic sediments. It constitutes a part of the Oman Ophiolite and is the largest exposure of oceanic lithosphere (Michibayashi et al., 2000). Intense structural studies in the region have revealed that a top-to-W shear dominates at the upper portion of the massif, i.e., above the crust-mantle boundary, whereas a top-to-E shear occurs at deeper levels (Ceulenner et al., 1988; Michibayashi et al., 2000; Dijkstra et al., 2002). Michibayashi et al. (2002) attribute conflicting shears to the variation in the relative velocity of the lithosphere and the underlying mantle flow (asthenosphere) to the spreading rate of the ridge.

The ~ NW-SE trending Makhbiyah shear zone (~ 20 km long, 1- 2 km wide) in the Wadi Tayin massif lies ~ 240 km SE to the Hilti massif. This shear zone exhibits an along-trend reverse shear i.e., top-to-NW in northern segment of the MSZ transitions and a top-to-SE to the south. Nicolas & Boudier (2008) propose that this shear reversal is not related to strike-slip faulting, but is rather related to the divergence of the asthenospheric mantle flow.

S.36 Nanga Parbat massif, Pakistan

The ~ N-S trending rocks of the Nanga Parbat massif, exposed at the western syntaxial bend of the Himalayan belt and to the south of the Main Mantle Thrust, represent the northernmost portion of the Indian plate. It is dominantly composed of high-grade schists and gneisses (Butler et al., 2000). The eastern margin of the massif shows a top-to-N (down) (brittle-ductile) shear overprint on top-to-S (up) (ductile) shear, and is considered to be a product of syn-convergent extension (Argles & Edwards, 2002).

S.37 Zanskar Shear Zone, India

The NE dipping Zanskar Shear Zone (ZSZ) lies in the NW Himalaya and constitutes an ~ 150 km segment of the South Tibetan Detachment System-Upper ($STDS_U$), which has also been referred to as the Zanskar Detachment in Gapais et al. (1992) and Searle et al. (1997). It is ~ 6 km thick, and lies in between the high-grade gneisses of the Higher Himalayan Crystallines (HHC) and the low-grade Tethyan Himalayan Sequence (THS) (Robyr et al., 2014). Around 35 km of ductile slip has been estimated along the ZSZ during the Early Miocene (Dèzes et al., 1999).

The ZSZ records two dominant phases of deformation corresponding to the contractional top-to-SW (up) followed by a top-to-N (down) normal fault-like extension. This shear reversal along the ZSZ has been reported by several workers (Mukherjee and Koyi 2010a, **Figs. S3a-d** in the supplementary file **S2**; review in Kellett et al., in press). Based on the U-Pb (zircon) and Pb-Th (monazite) ages of the granitic bodies from the HHC, Gehrels et al. (2003)

postulate that the top-to-N thrust motion along the South Tibetan Detachment initiated during Cambro-Ordovician times. The authors, however, did not specify if it were $STDS_L$ or $STDS_U$. With the help of U-Pb dating of monazites, Finch et al. (2014) suggest that the inversion in slip sense occurred during ~ 26 – 22 Ma, and that the top-to-N (down) shearing terminated ~ 20 Ma. However, the data compiled in Carosi et al. (2018) reveal a much younger age ~ 13-11 Ma for the STDS activity in Western Bhutan. Finch et al. (2014) also calculate that ~ 24 km normal displacement had taken place within ~ 6 Ma. Top-to-the-NE shear occurred in the $STDS_L$ from 24 - 12 Ma and in the $STDS_U$ from 19 - 14 Ma (review in Godin et al. 2006). Switch in shear sense in ZSZ has been explained in terms of a first top-to-S compression induced by India-Eurasia collision, and a subsequent combined simple shear and Poiseuille flow of the HHC materials (Mukherjee and Koyi 2010a). Subsequently, a Poiseuille flow in combination with critical taper mechanism of deformation has also been conceived from numerical models (Beaumont et al. 2010) and field-studies (Mukherjee 2013a) in general for the HHC.

{Insert Figure S3 about here}

S.38 Tso Morari Crystallines, Ladakh, India

Northward subduction of Indian plate beneath Eurasian has produced UHP eclogite facies metamorphic units in the Tso Morari area (NW India) (Palin et al., 2017 and references therein). The Tso Morari Crystallines (TMC) crops out south to the Indus Tsangpo Suture Zone (ITSZ) with a sub-elliptical outline (dimension: ~ 100 * 50 * 7 km^3) (Mukherjee & Mulchrone, 2012). Gneissic rocks, meta-sedimentary units and granitoids constitute the major components of the TMC. Previous authors viz. Guillot et al. (1997), de Sigoyer et al. (2004), Epard & Steck (2008), report at least three deformation phases for the TMC. This region has undergone insignificant erosion (Yin, 2006).

Dutta (2016), based on meso-scale quartz fish and winged inclusions briefly report the presence of both top-to-N and top-to-S ductile shears (**Figs. S3e,f** in the supplementary file **S2**). Sen et al. (2013), on other hand, claim that the Zildat Detachment fault, which marks the northern boundary of the TMC, reactivated as a thrust (top-to-SW (up)) after an initial syn- and post-exhumational top-to-NE (down) slip. The southern margin of the TMC, known as the Karzok fault, which sheared top-to-SW (down) (de Sigoyer et al. 2004), possibly underwent a late reverse shear (top-to-NE (up)) as shown by the focal mechanism solutions (Hazarika et al., 2017).

S.39 North Almora Thrust Zone, India

The ~ 6 km thick and S-dipping North Almora Thrust Zone (NATZ) demarcates the ~ WNW-ESE trending Almora Crystalline Complex (ACC) or the Almora klippe that constitutes the Lesser Himalayan Sequence (LHS) in the north. The rock types in the NATZ are mainly mylonitic schists and gneisses metamorphosed up to the amphibolite facies (500 – 600 °C), although the rocks mylonitized under greenschist facies (400 – 500 °C) (Srivastava & Mitra, 1996; Joshi et al., 2017). The mylonites close to the NATZ exhibit both top-to-N and top-to-S shear senses, both ductile and brittle. Agarwal et al. (2016) propose that the NATZ reactivated as a back-thrust i.e., the shear sense reversed from top-to-S to top-to-N, after the ACC emplaced. However, the authors did not cite any reason for the reversal of the slip sense. OSS has also been reported from the Sarayu Formation of the Almora Nappe (NW Himalaya, India) by Joshi (1999), but the poor quality of the thin-section image (fig. 4a) renders it difficult for re-interpretation by other workers.

S.40 Tethys Himalaya, Tibet

The Tethys Himalaya, at southern Tibet, lies in between the Great Counter Thrust (GCT) to the north and the South Tibetan Detachment System-Upper ($STDS_U$) to south, and extends for > 1500 km along the Himalayan Arc. Both the GCT and the $STDS_U$ strike ~ NW-SE. The Tethyan Himalaya is composed primarily of the un-/weakly metamorphosed sediments of the now dissappeared Tethys ocean. There are scattered occurrences of HP gneiss domes within the Tethyan belt: towards E- Malashan, Lhagoi-Kangri, Mabja, Kampa, Kangmar etc. (fig. 1 of King et al., 2011). The structural evolution of the Tethys Himalaya is quite complex, because of the overprinting of the syn-collisional (top-to-S) compressional structures by north-directed extensional features owing to the top-to-N (up) slip on the southerly dipping GCT followed by orogen-parallel extension (post 18 Ma), which formed ~ NE-SW trending shear zones and normal faults viz., Thakkola graben, Tingri graben, Ama Drime detachment (Langille et al., 2014 and references therein).

Langille et al. (2010) study the mid-crustal rocks (gneisses and schists) of the Mabja Dome that dominantly show top-to-S shear (S-C shear fabrics, quartz CPO, σ-type porphyroblasts etc.) at structurally lower levels. However, equally numerous top-to-N and top-to-S shears are found (**Fig. S3b** in the supplementary file **S2**), without any cross-cutting relation, in the structurally higher lithounits. The authors suggest this to be result of either heterogeneous viscosity or bulk pure shear during exhumation. King et al. (2011), on the other hand, report overprinting relation between the S-C fabrics exhibiting top-to-N and top-to-S shear senses at the granite gneiss – Tethyan sequence contact and conclude that the former occurred later at lower grade (greenschist facies) conditions. This top-to-N shear is the dominant shear away from the contact.

{Insert Figure S4 about here}

S.41 Kathmandu Nappe, Nepal

The Kathmandu Nappe in the central Nepal Himalaya overlies the Lesser Himalayan rocks separated by the Mahabharata Thrust (< 22 Ma, out of sequence thrust; Mukherjee, 2015b and references therein) equivalent to the Main Central Thrust – Upper (MCT_U). The ~ ENE-WSW trending nappe mainly consists of schists, marbles, quartzites, with the grade decreasing up-section (Guillot, 1999).

Bell & Sapkota (2012) identify under an optical microscope at least four deformation phases based on the matrix-foliation relations from within the garnet porphyroblasts, with possible reversal in the shear senses from top-to-N to top-to-S. The authors suggest that this could be by repeated crustal thickening and gravitational collapse that moved rocks across the orogen core (zone of maximum horizontal shortening), thereby exhibiting bidirectional shear (**Fig. 22**).

S.42 Gavilgarh–Tan shear zone (GTSZ), India

The dominantly ductile, ~ ENE-WSW trending ~ 120 km long GTSZ crops out in between the Sausar and the Betul supracrustals belts, Central India. It forms the southern margin of the ~ ENE-WSW trending Central Indian Tectonic Zone (CITZ). The GTSZ primarily consists of mylonitic granitoids and gneisses and pseudotachylytes (Chattopadhyay & Khasdeo, 2011). The pseudotachylytes preserve signatures, at both meso- and micro-scales, of two episodes of '*geometric*' reactivations (Holdsworth et al., 1997) and shear reversals within the GTSZ: ductile sinistral (core-mantle structures , quarter structures, both σ- and δ-porphyroclasts of

K-feldspars, and S-shaped folds) → ductile - semi-brittle dextral (aligned mica fish, oblique foliations, shear bands) → brittle sinistral (domino structures) (Chattopadhyay et al., 2008). Although Chattopadhyay et al. (2008) identify the temporal relationships between the deformations, they did not state the cause for the reactivation.

S.43 Eastern Ghats Belt, India

The ~ NE-SW trending Eastern Ghats Belt (EGB) is an arcurate, intensely deformed Precambrian gneiss-granulite UHT terrane. It extends along the eastern coast of India for ~ 600 km. Its width decreases from the north (~ 100 km) to the south (~ 20 km) (Sharma, 2009 and references therein). Dobmeier & Simmat (2002) report ~ NE-SW trending strike-slip shear zones in the Chilka Lake area (NE part of the EGB), which exhibit both dextral (dominant) and sinistral slip sense. However, neither the temporal relations nor the origin of OSS has been stated.

S.44 Achankovil Shear Zone (AKSZ), Southern India

This ~ NW-SE trending shear zone extends ~ 150 km within the Southern Granulite Terrain (SGT). It is ~ 30 km wide, and separates the charnockites and gneisses of the Maduarai block to the north from the khondalites and migmatites of the Trivandrum block to the south. The rocks from both these crustal blocks belong to the Archean (3 – 2 Ga), whereas the charnockites, quartzofeldspathic gneisses of the AKSZ are much younger (1.5 – 1.3 Ga) (Harris et al., 1994; Rajesh et al., 1996; Ghosh et al., 2004).

The highly strained AKSZ underwent at least three phases of deformation between 2500 – 550 Ma (U-Pb Zircon geochronometry, Ghosh et al., 2004), and exhibit ~ NW-SE trending steep to sub-vertical foliations with sub-horizontal lineations connoting transpression.

Mesoscopic evidences viz. S-shaped folds, asymmetric boudins, shear bands etc., for both sinistral and dextral deformations have been reported from the AKSZ (Sacks et al., 1997). Rajesh & Chetty (2006), based on field studies as well as utilizing remote sensing images and SRTM data, confirm overprinting of a ductile dextral deformation by late stage brittle-ductile sinistral shear. The authors further relate them to D2 and D3 deformations of the East African (750 – 620 Ma) and Kuunga (570 – 550 Ma) orogens, respectively.

S.45 Thai Peninsula, Thailand

The Thai Peninsula lies to the east of the ~ N-S trending Sunda Trench (also known as the Java Trench), which marks the subduction of the Australian plate beneath the Eurasian plate. The internal deformation of the Thai Peninsula is characterized by two ~ N-S trending strike-slip faults viz. the Rangong Fault (RF) and the Khlong Marui Fault (KMF). These faults along with the ~ NW-SE trending Mae Ping Fault (MPF) and the Three Pagodas Fault (TPF) played crucial roles in defining the tectonic history of South East Asia (Tapponnier et al., 1986; Gilley et al., 2003). The sense of slip along the TPF and the MPF reversed from sinistral (ductile) to dextral (brittle), supposedly due to the India-Eurasia collision (Tapponnier et al., 1986) ~ 55 Ma back (Najman et al., 2017). The KMF and the RF also reversed shear from dextral to sinistral (~ 52 Ma, Ar-Ar dating of muscovites in granites pre-kinematic to this reversal, by Chârusiri, 1993). Lacassin et al. (1997) propose Indo-Asia collision as the cause, however, Watkinson et al. (2008) point out that the subduction along the southern Sundaland resulted in the brittle reactivation of the KMF and the RF.

S.46 Red River Fault Zone (RRFZ), China

The ~ 80 km thick RRFZ, also known as the Ailao Shan Red River shear zone (~ NW-SE trending), is a major strike-slip fault system in southeast China. It can be traced for > 1000 km from Tibet to the South China Sea (Zhu et al., 2009 and references therein). The tectonic evolution of the RRFZ is best described by a two-stage extrusion model of Tapponnier et al. (1986), which also explains the slip reversal from sinistral (~ 32–16 Ma, Ar-Ar dating of micas, amphiboles and K-feldspars by Leloup et al., 2001) to dextral (post-16 Ma). By ~ 16 Ma the eastward extrusion of the Indochina block had ended. However, continued collision of the Indian and Eurasian plates triggered extrusion of the South China block to the east relative to the Indochina block and thereby resulted in the late-stage shear reversal of the RRFZ (Leloup et al., 2001).

S.47 Beishan Terrane, China

The Paleozoic Beishan terrane lies at the southern part of the Central Asian Orogenic Belt (CAOB), NW China. Apart from the Proterozoic metasedimentary sequences, it also comprises of intensely folded and refolded Permian turbidites that record the Late Permian-Jurassic intraplate deformation of the central Asia (Xiao et al., 2010; He et al., 2018; Stern et al., 2018). These folded rocks are bounded by three strike-slip faults viz. Pochengshan Fault (PF) to the north, Xinxingxia Fault (XF) to the west and Southern Bounding Fault (SBF) to the south. The ~ E-W trending PF and SBF reversed slip sense from sinistral-oblique (Late Triassic) to dextral-oblique (Middle-Late Jurassic). The reason of this reversal is debated. Darby & Ritts (2007) suggest this reversal was partly triggered by the collision between the Qingtang and Lhasa terranes along the Bangong-Nujiang suture. However, Baxter et al. (2009) report that this collision took place in the Createceous and not in the Middle-Late Triassic as claimed by Darby & Ritts (2007). Zhang & Cunningham (2012) believe that clockwise rotation of the Siberian cratons with respect to that of the North China craton produced Late-Triassic ~ NE-SW directed horizontal shortening, and westward subduction of Pacific plate beneath the Eurasian plate along eastern China reoriented the horizontal compression direction to ~ NW-SE, which in turn caused the reversal in Middle-Late Jurassic.

S.48 Ertix fault, China

The NW-SE trending Ertix fault lies within the Central Asian Orogenic System (> 1000 km wide, > 4000 km long), and marks the southern boundary of the ~ 600 Ma old Altaids (Wilhem et al., 2012). The > 2500 km long fault continues from NW China to SW Mongolia (Briggs et al., 2007 and references therein; Stern et al., 2018). Intra-continental deformation, which is widespread in Central Asia (Raimondo et al., 2014), reversed the shear sense from dextral to sinistral (Mid-Late Paleozoic) along the Ertix fault, which in turn produced the Junggar Basin. The same was inferred from the arrangement/deflection of dyke swarms, faults and the trend of the pull-apart basins in the vicinity etc (Allen et al.,1995; Han & Zhao, 2018).

S.49 Tan-Lu fault, China

Around NNE trending Tan-Lu fault can be traced along the eastern China for > 3600 km from the Dabie-Shan terrane to the Liaodong Bay in the north. It is considered one of the longest continental strike-slip faults (Jiawei & Guang, 1994), with abundant ~ 165 – 110 Ma (U-Pb zircon geochronology of granites) magmatic rocks, viz., andesite, basalt, rhyolite etc. distributed along its length (review in Wang et al., 2018). The presently seismic Tan-Lu fault (Li & Hou, 2019) has accommodated > 500 km sinistral slip since its initiation ~ 210 Ma ago (U-Pb dating of UHP eclogites) as the South and the North China blocks collided (Ames et al., 1993; Yin & Nie, 1993; Zhao et al., 2017; Meng et al., 2019). However, the slip sense reversed after the Mid-Mesozoic. 2D and 3D seismic studies conducted by Hsiao et al. (2004) find out positive and negative flower structures associated with the Tan-Lu fault. The authors notice that the timing of slip reversal is coeval to the *(i)* Indo-Asia collision, and *(ii)* change in subduction direction from NW to W (Northrup et al., 1995) of the Pacific plate beneath the Eurasian plate. Hence, these two events might have caused the reversal to dextral-slip along the Tan Lu fault.

S.50 Chungnam Basin, South Korea

This basin lies within the Korean Peninsula to the east of the ~ NNE-SSW trending, ~ 100 km long Dangjin Fault (Devonian – Mid-Jurassic). The majority of the structures in this Basin developed in response to the two phases of deformation of the Daebo Orogeny viz., *(i)* ~ 170 – 160 Ma WNW-ESE compression, followed by *(ii)* ~ 150 Ma N-S shortening (Chough et al., 2000 and references therein). Sinistral displacement along the Tan Lu Fault (Section 4.31) may have contributed to the latter.

Lim & Cho (2012) report close-spaced OSS (shear bands, oblique foliations, asymmetric folds etc. identified from the outcrop) from the Chungnam Basin. The authors propose a tectonic model wherein the westward transport of rocks during the ~ WNW-ESE shortening coupled with tilting and overturning of the deforming rocks (**Fig. 21**) developed the OSS.

S.51 Yamasaki, Mitoke fault zones and Median Tectonic Line, Japan

The ~ NW-SE trending Yamasaki and Mitoke active strike-slip fault systems (YFZ, MFZ) are exposed within the "*inner belt*" of SW Japan that is bounded to the south by the ~ ENE-WSW striking and ~ 1000 km long Median Tectonic Line (MTL) (Maruyama & Lin, 2004). The epicenters of the 1968 (M 5.6) and 1984 (M 5.6) lie within the MFZ and the YFZ, respectively. Moreover, the ~ 80 km long YFZ consists of several sub-parallel ~ 10 to 35 km long faults, and is still considered to be one of the most seismically active fault zones capable of generating large earthquakes in SW Japan (Nugraha et al., 2013). Watanabe et al. (1996) further show that seismicity of the YFZ re-initiated after the Kobe earthquake (1995, M 6.9). The MFZ, on the other hand is ~ 50 km long and consists of three major strike-slip faults: towards north, Habu, Tonoda, and Mitoke. The YFZ, MFZ and MTL are primarily composed of fault-breccias, mylonites and cataclasites.

Based on the deflected geometry of the rivers and quaternary terraces in the vicinity of the fault zones, as well as from the asymmetric shear fabrics viz. S-C planes, Riedel shears, drag folds etc., recorded in the fault zone rocks, Maruyama & Lin (2004) confirm Late Miocene shear reversals viz., dextral → sinistral for YFZ and MFZ, and sinistral → dextral along the MTL. Paleomagnetic studies carried out by Otofuji et al. (1991) reveal a Mid-Miocene clockwise ~ 45° rotation of SW Japan with respect to the eastern Eurasia. Yamamoto (1991) studies the orientations of the fractures and dike swarms to show that the directions of maximum horizontal stress in SW Japan changed from N-S/ NE-SW to NW-SE/WNW-ESE in the Late Miocene, possibly due to the opening of the Japan Sea. The present stress orientation in the region i.e. ~ NW-SE/WNW-ESE proposed by Heidbach et al. (2018) matches to that given by Yamamoto (1991). Maruyama & Lin (2004) propose that this switch in the horizontal stress axes reversed the slip sense along the fault zones in the SW Japan.

S.52 D'Entrecasteaux Islands, Papua New Guinea

The ~ WNW trending D'Entrecasteaux Islands lie to the north of the Papuan orogen, which resulted as the Australian plate collided with an island arc terrane to the north during the Eocene. The islands occupy a central position within the submerged Woodlark rift, with a present day spreading rate of ~ 20 - 42 mm yr^{-1}, lies in between the Woodlark microplate and the Australian plate (Little et al., 2011; Holm et al., 2016 and references therein). These islands host the youngest (~ 2–8 Ma, U-Pb ages of zircons, Ar-Ar ages of micas and amphiboles) (U)HP eclogite facies rocks, which were previously a part of the Australian continental crust that subducted to > 100 km depth, and later exhumed to the Earth surface at > 2 cm yr^{-1} as several diapirs (Little et al., 2011).

EBSD-based quartz CPO studies conducted by Little et al. (2013) on the gneissic hosts of the eclogitic rocks, document OSS (top-to-NE and top-to-SW) (**Figs. S3c1,c2** in the supplementary file **S2**) from rock samples that were merely about a meter apart in the field. Little et al. (2011) report bi-directional shear (top-to-E and top-to-W) also exhibited by micro-scale conjugate shear bands, mica fish, asymmetric feldspar porphyroclats etc. The authors conclude that the reverse shears are syn-exhumational and originated by coaxial deformation.

S.53 Woodroffe thrust, Australia

The E-W trending Woodroffe thrust, over which the hanging wall rocks slipped > 60 km, is a > 600 km long and > 1.5 km wide mylonitic shear zone within the Proterozoic metamorphic rocks of the Musgrave Block in central Australia (Wex et al., 2017, 2018). Apart from the mylonites that swerve around less deformed granitic/gneissic bodies, the Woodroffe Thrust, also consists of numerous pseudotachylyte veins (Lin et al., 2005).

The asymmetry of the quartz CPO fabrics obtained from the mylonitc rocks using pre-mylonite grains show both top-to-N and top-to-S shear **(Figs. S3d1,d2** in the supplementary file **S2**) (Bell & Johnson, 1992 and references therein). However, regional field studies carried out by Bell & Johnson (1989) indicate a top-to-N thrusting of the granulitic over amphibolite facies rocks. Although the authors discuss and clarify the errors in interpreting shear senses from asymmetric kinematic indicators, they do not explain the conflict in shear senses shown by the quartz c-axis plots, which they encountered.

S.54 Mary Kathleen fold belt, Australia

The ~ N-S trending > 80 km long Mary Kathleen fold belt (MKFB) crops out near the center of the Proterozoic Mt. Isa inlier. It consists of intensely deformed igneous (gabbro, granite) and metasedimentary rocks (metaquartzites, metasiltstones) (Oliver et al., 1994; Neumann et al., 2009). The MKFB represents an initially sub-horizontal shear zone with either top-to-S (Pearson et al., 1992) or top-to-N (Holcombe et al., 1991) shear in the mylonites. E-W compression subsequently folded this shear zone.

Holcombe et al. (1991) report that the E verging limb of the fold exhibit both top-to-N and top-to-S shears. However, the shear senses obtained from quartz CPO studies and oblique quartz shape fabrics do not match with those shown by the S-C fabrics in the W-verging limb, possibly due to localized shear reversals. The authors also propose folding-induced shear reversal in the E-dipping limb.

S.55 Castle Cove Fault (CCF), Australia

This ~ 30 km long NW dipping near-vertical fault lies within the eastern part of the NW-SE trending Otway Basin in SE Australia. The basin, with a ~ 10 to 13 km thick Jurassic - Cenozoic sedimentary sequence, originated during the Late Jurassic separation between the Australian and Antarctica plates, and is spread over ~ 1.5×10^5 km^2 in the onshore and the offshore of SE Australia (Stacey et al., 2013). 2D seismic studies and subsurface mapping of unconformities along with biostratigraphic data reveal that the CCF originated as a normal fault during the NW-SE extension-induced Late Cretaceous rifting. This was followed by a Late Miocene NW-SE compression, which continues till the present (Rajabi et al., 2017), reactivating the CCF as a reverse fault and folding the hanging wall rocks into a large anticline of ~ 80 m wavelength (Holford et al., 2014; Debenham et al., 2018).

S.56 Moonlight Fault Zone (MLFZ), New Zealand

The steeply dipping, ~ NE-SW trending MLFZ (sub-parallel to the Alpine Fault to the east) are exposed for > 300 km at the South Island (eastern New Zealand), to the west of the Otago Fault System. MLFZ rocks - quartzofeldspathic schists, cataclasites and breccias (towards the fault core) – underwent a peak metamorphism at lower greenschist facies (~ 300 °C) (Alder et al., 2016). Turnbull et al. (1975), based on field and petrographic studies, identify that the MLFZ formed as an extensional fault during the Early Oligocene. However, ~ NW-SE compression during the Miocene reactivated it as a reverse fault and consequently, exposed deep seated rocks (Norris et al., 1978, 1990) (Positive Inversion: Section 4.2.1). Smith et al. (2017) conduct *"frictional sliding experiments"* on MLFZ rocks using biaxial deformation equipment (Collettini et al., 2014) and reveal that this inversion along the Moonlight Fault was facilitated by fluid-induced frictional weakening of the rocks.

SUPPLEMENTARY FIGURES & CAPTIONS (S2)

Fig. S1. Locations of the terranes from **Table I** (first referred in Section 1 in the main text). The numbers within squares indicate the corresponding 'Sl.no.' in **Table I**. Red circles: ductile; Blue stars: brittle.

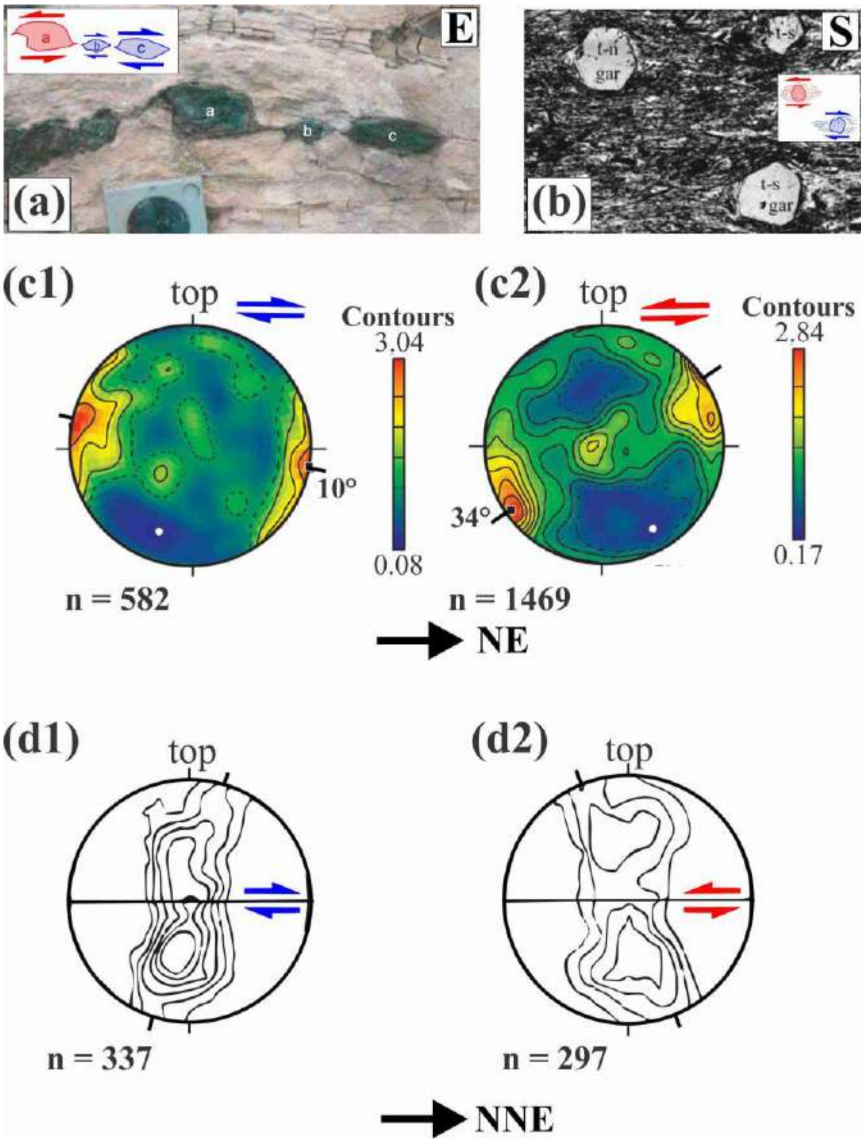

Fig. S2. OSS reports from the literature (first referred at Section S.8). **(a)** Train of asymmetric boudins. Both top-to-W (boudin a) and top-to-E (boudins b, c) are present (reproduced from fig. 9b of Cooper et al., 2010; location: Northern Snake Range Mylonite Zone, USA (location #8 in **Fig. 24a**)). (b) Garnet porphyroclasts from the schist of Mabja Dome (width of view: 6 mm) (S Tibet) exhibit both top-to-N and top-to-S shear senses (reproduced from fig. 6b of Langille et al., 2010; location #40a in **Fig. 24c**). Quartz CPO plots of two different samples **(c1)** PNG-09-008a, and **(c2)** PNG-09-008b from the same outcrop in the D’Entrecasteaux Islands, Papua New Guinea (location #52 in **Fig. 24a**) showing opposite shear senses (reproduced from Appendix C of Little et al., 2013). **(d1,d2)** Quartz CPO plots from the mylonites of the Woodroffe Thrust Zone, Australia (location #53 in **Fig. 24a**) (reproduced from fig. 1 of Bell & Johnson, 1992). ‘n’ denotes the number of c-axis plotted. Inset figures in **(a)** and **(b)** show the corresponding sketches.

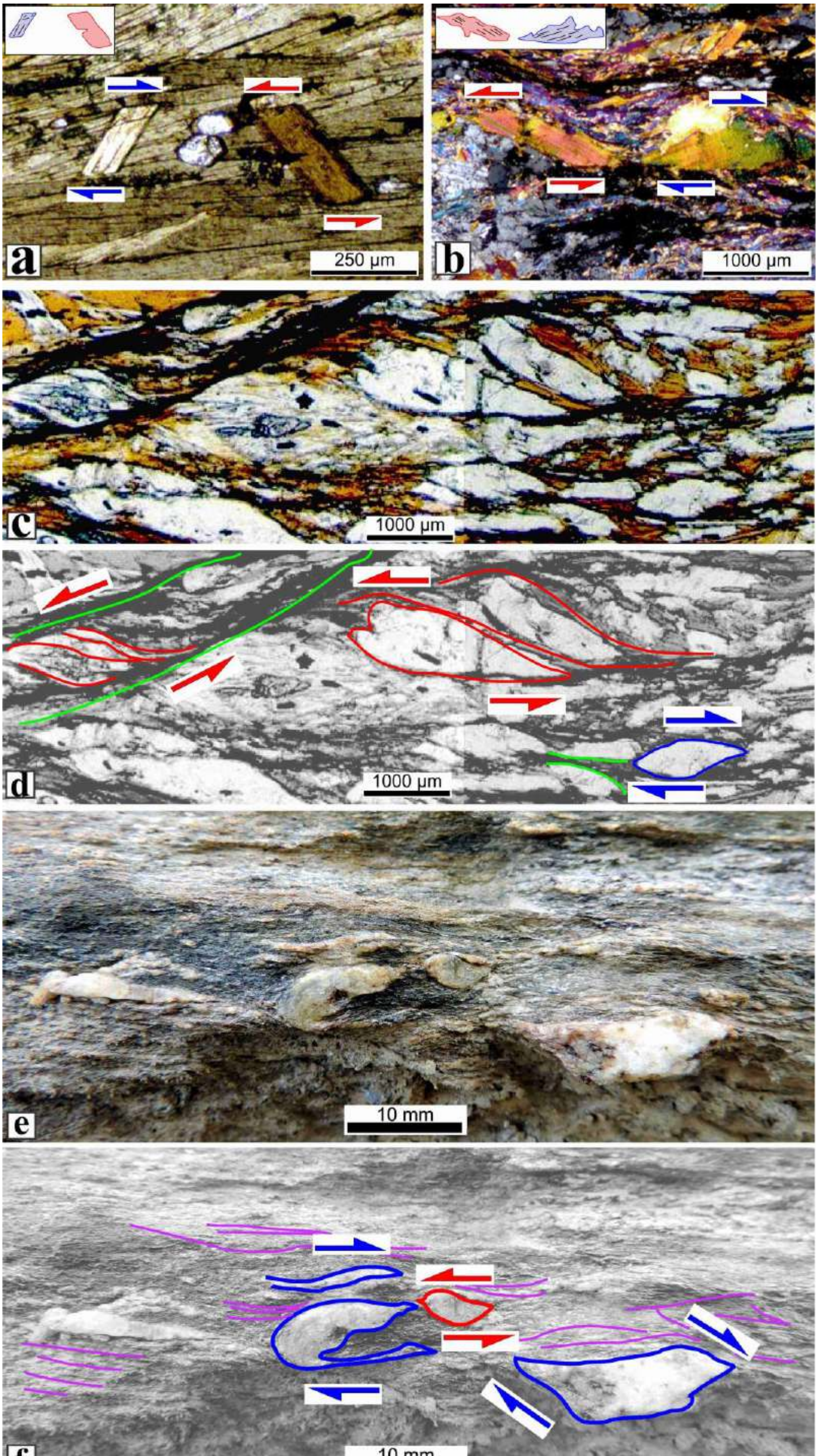
a
250 µm
b
1000 µm
c
1000 µm
d
1000 µm
e
10 mm
f
10 mm

Fig. S3. Ductile OSS at micro-scale (first referred at Section S.37). Parallelogram shaped **(a)** mica grains and **(b)** mica fish exhibiting both dextral (blue half arrows) and sinistral shear (red half arrows) (reproduced from figs. 1.85 and 6.7 of Mukherjee, 2013b). **(c,d)** S-C fabric and asymmetric quartz grains in the mylonitic sample show top-to-left and top-to-right shear (red and blue half arrows, respectively). **(e,f)** Winged inclusion at the centre and quartz fish at lower right corner show top-to- right shear (blue half arrows), whereas sigmoid quartz clast at the centre exhibits top-to-left shear (red half arrows). **(d)** and **(f)** are gray-scale versions of **(c)** and **(e)**, respectively. Locations: **(a,c,d)** Zanskar Shear Zone (Western Himalaya, India), **(b,e,f)** Tso Morari Crystallines (Ladakh Himalaya, India).

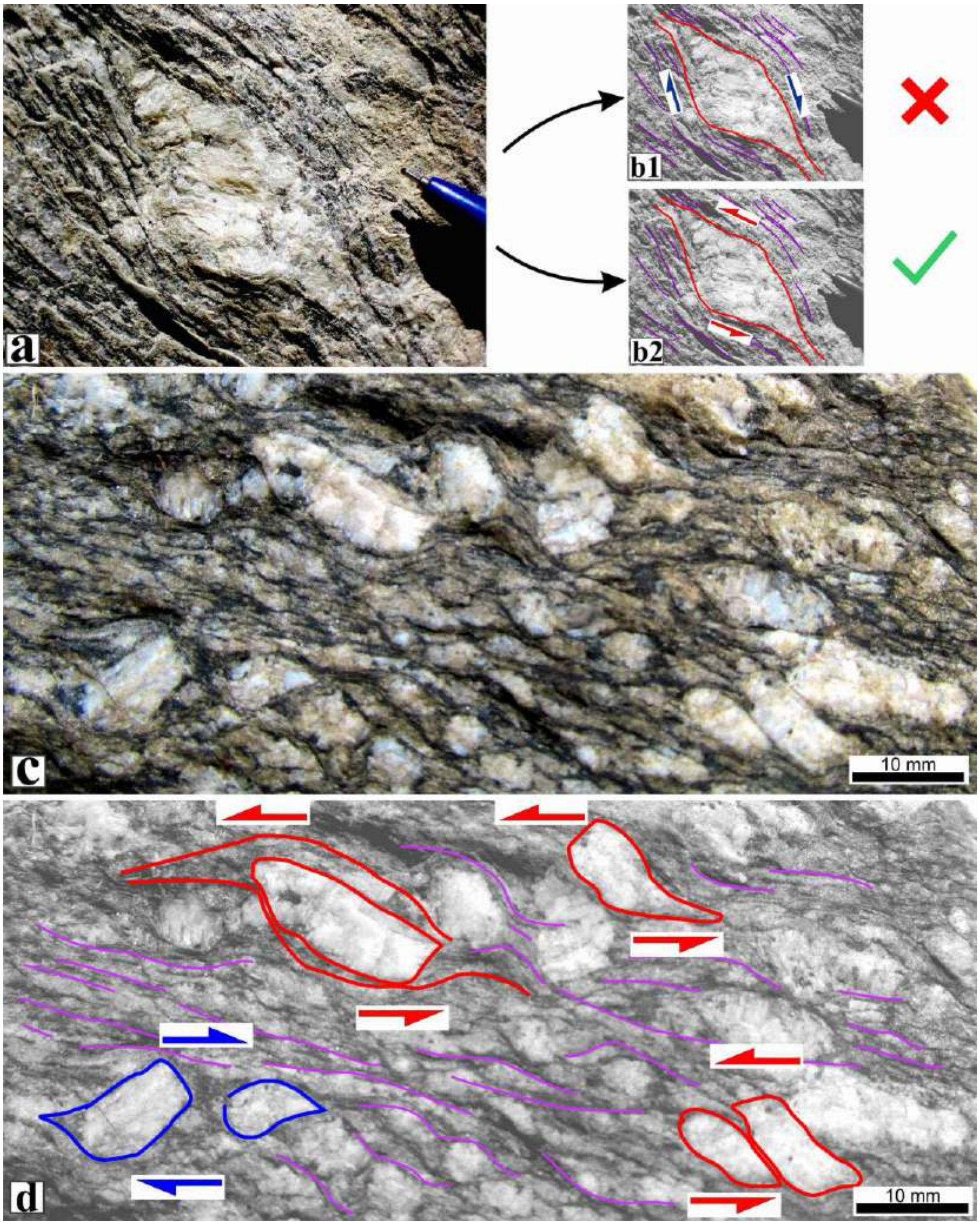

Fig. S4. Reports of OSS from Indian Himalaya. **(a)** Parallelogram shaped quartz pod. Both the misinterpreted **(b1)** and correct **(b2)** shear senses are shown. Note that the shear sense has been deduced using the orientation of the foliations around the pod (reproduced from fig. 1.41 of Mukherjee, 2014b). Compare with **Fig. 8e1. (c,d)** OSS in mylonitized gneissic sample with sigmoid shaped quartz clasts. Locations: **(a-d)** Bhagirathi section, Higher Himalayan Crystallines (Uttarakhand state, India). **(d)** is the gray-scale version of **(c)**.

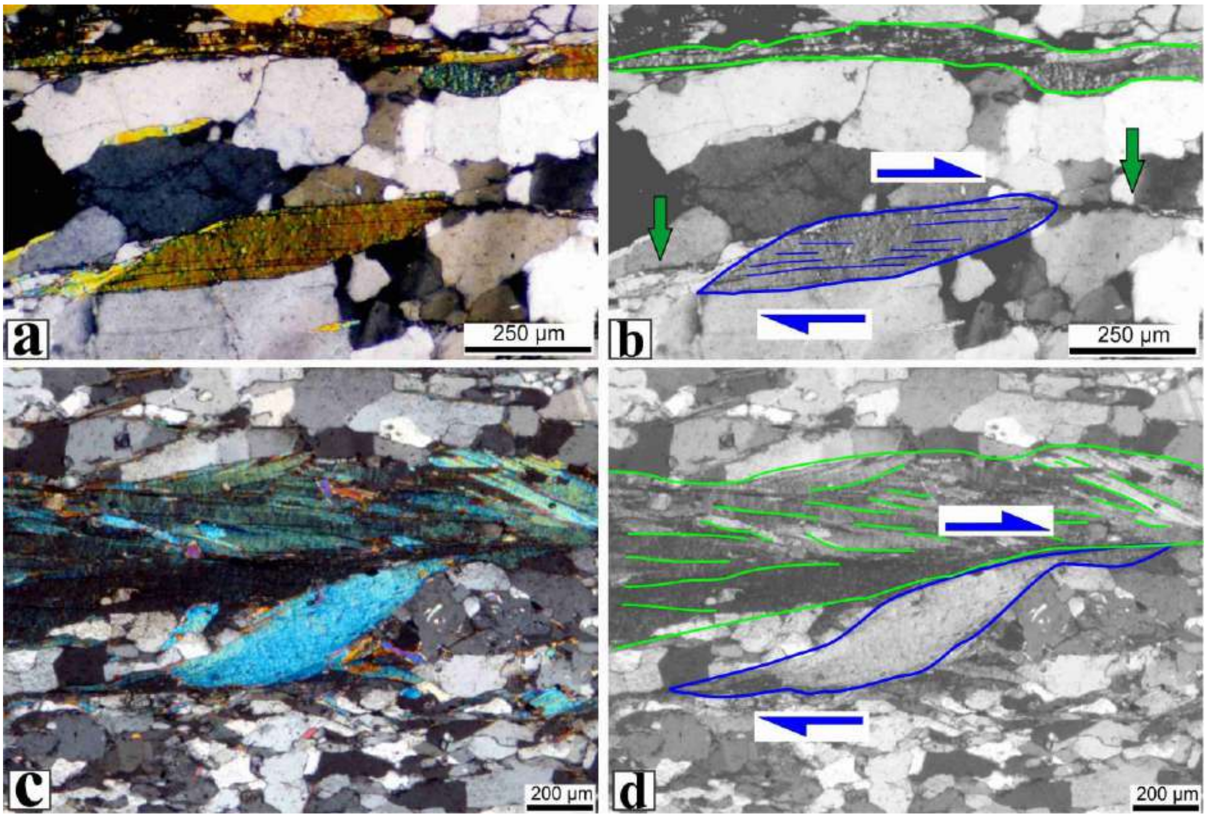

Fig. S5. Ductile shear sense indicators (first referred at Section 1 in the main text). **(a,b)** Parallelogram shaped mica fish with cleavage planes parallel to the C-plane. Sense of shear is dextral. Note the orientation of foliation (green full arrows) that has been used in deducing the shear sense (reproduced from 1.56 of Mukherjee, 2013b). **(c,d)** Sigmoidal muscovite fish. **(b)** and **(d)** are gray-scale versions of **(a)** and **(c)**, respectively. Dextral shear sense is perfectly clear from the shape of the fish. Locations: **(a,b)** Karakoram Shear Zone, **(c,d)** Tso Morari Crystallines (Ladakh Himalaya, India).

Fig. S6. Google Earth derived cross-section along the ABC transect of **Fig. 25** (first referred in the caption of **Fig. 25**).

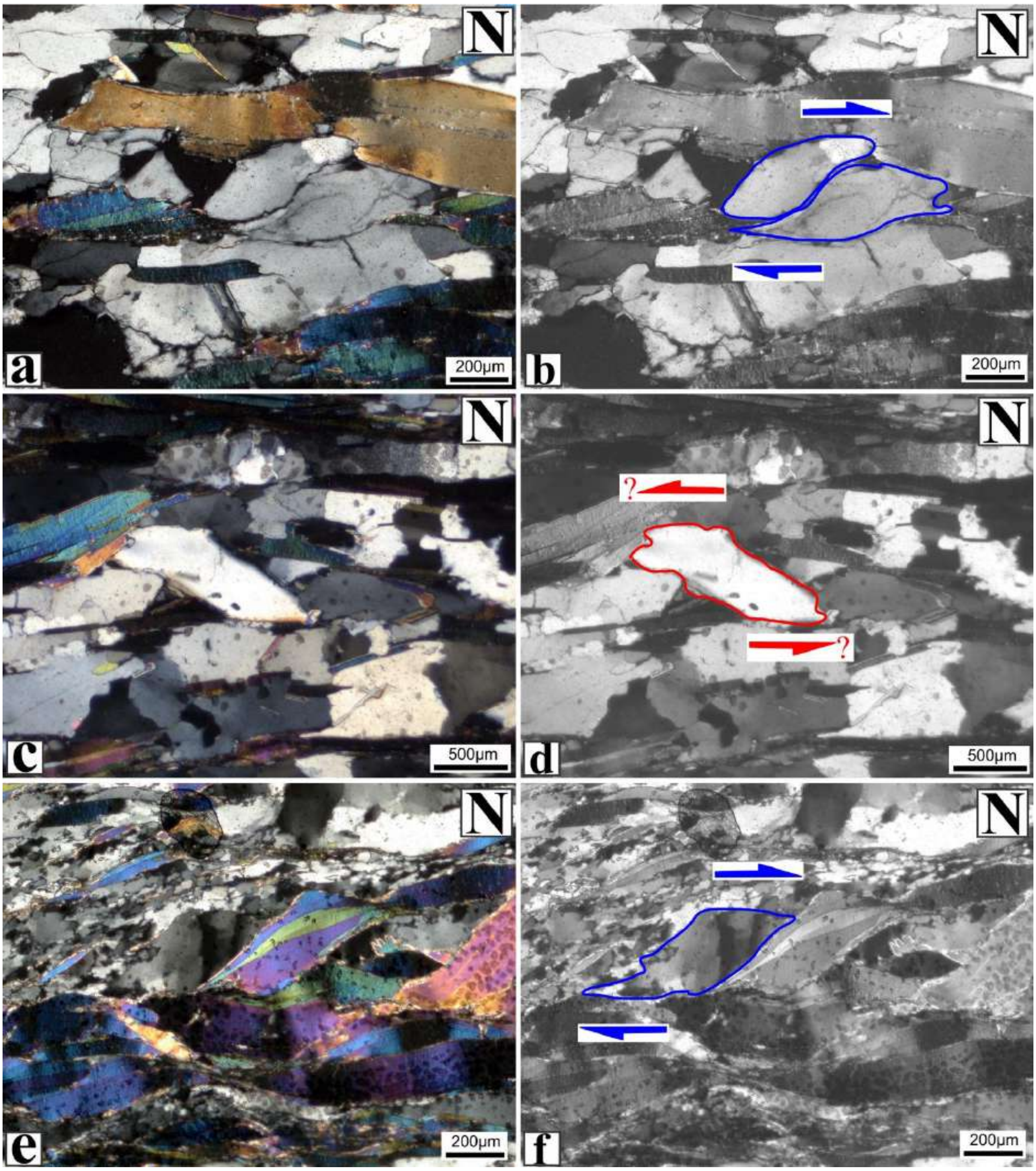

Fig. S7. Ductile shear sense indicators from Chaura region (**Fig. 25**) (NW Himalaya, Uttarakhand state, India) (first referred at Section 6.2 in the main text). **(a,b)** Top-to-right (N) indicated by the two sigmoidal quartz fish, **(c,d)** Probable top-to-left (S) shear sense shown by the near-parallelogram shaped quartz grain, **(e,f)** Top-to-right (N) shear sense is exhibited by both the sigmoidal quartz fish and the sigmoidal muscovite to the right. The primary shear plane for all the images is horizontal. (b), (d), and (f) are gray-scale versions of (a), (c), and (e).

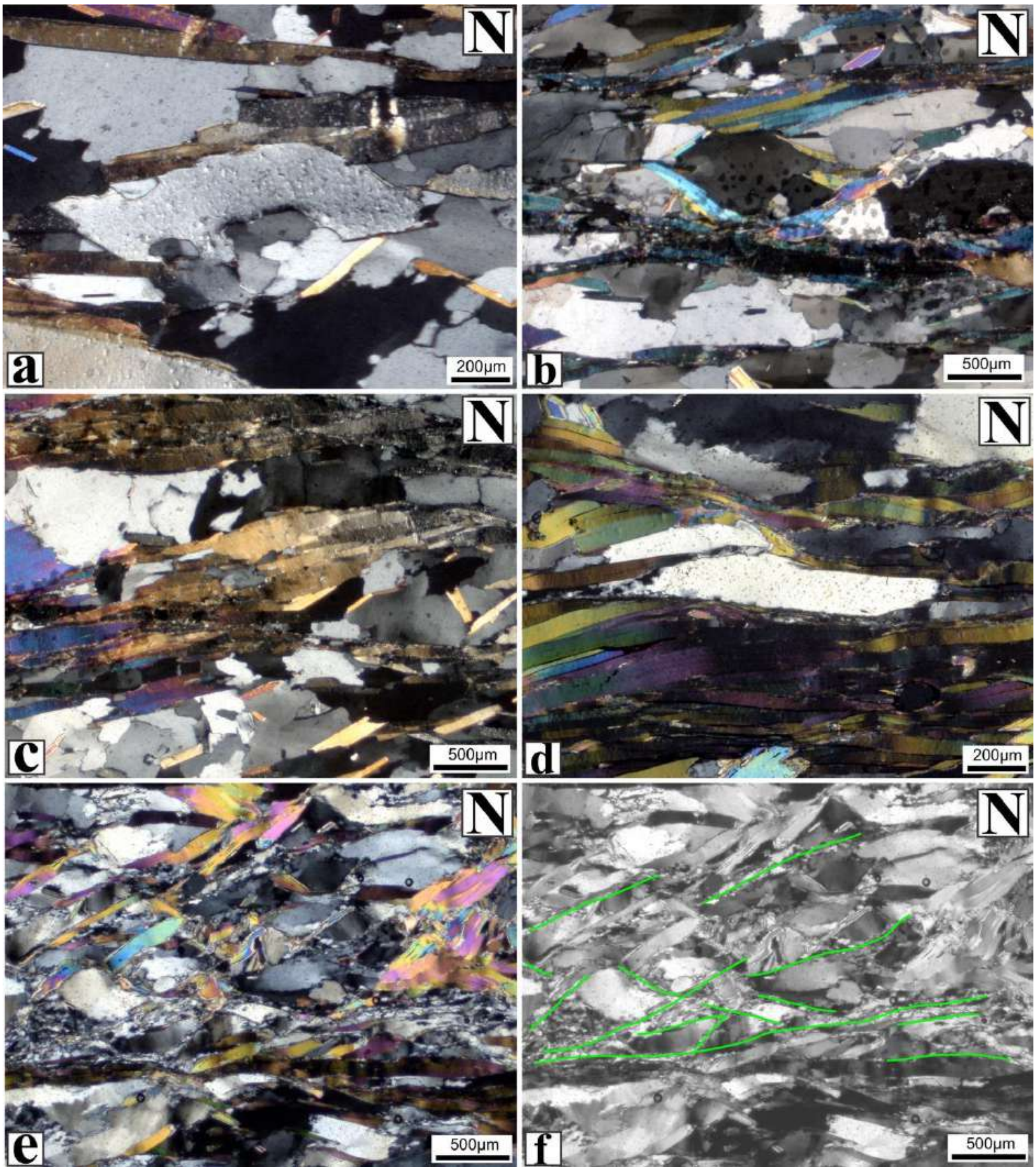

Fig. S8. Unreliable shear sense indicators from the schistose rocks of the Chaura region (**Fig. 25**) (NW Himalaya, Uttarakhand state, India) (first referred at Section 6.2 in the main text). **(a)** An irregular-shaped quartz grain (center). The quartz grains from below have migrated into it resulting in the jagged margin. Although the long axis of the grain at the center is tilted and the lateral margins are crudely sigmoid, such grain should be avoided in deciphering the shear sense. **(b)** Symmetrical quartz grain surrounded by muscovite grains. It does not indicate any shear sense and hence must be avoided. (c) The aggregate of muscovite grains (foliation fish, **Fig. 1j**) exhibit a top-to-right (N) shear. However, the quartz grains above and below do not show similar geometry. **(d)** Overlap between the quartz grain (center) and the surrounding muscovite and biotite seem to have resulted in a trapezoidal shape (Mukherjee, 2012a) of the former (see **Fig. 7d1**), and hence in such cases care should be taken before deciding the shear sense. **(e,f)** Intensely deformed portion of a rock may exhibit such complex intersections of shear planes/zones making it difficult to differentiate the antithetic shear planes from the synthetic shear planes of different deformation stages in case of shear reversal, if any. **(f)** is a gray-scale version of **(e)**.

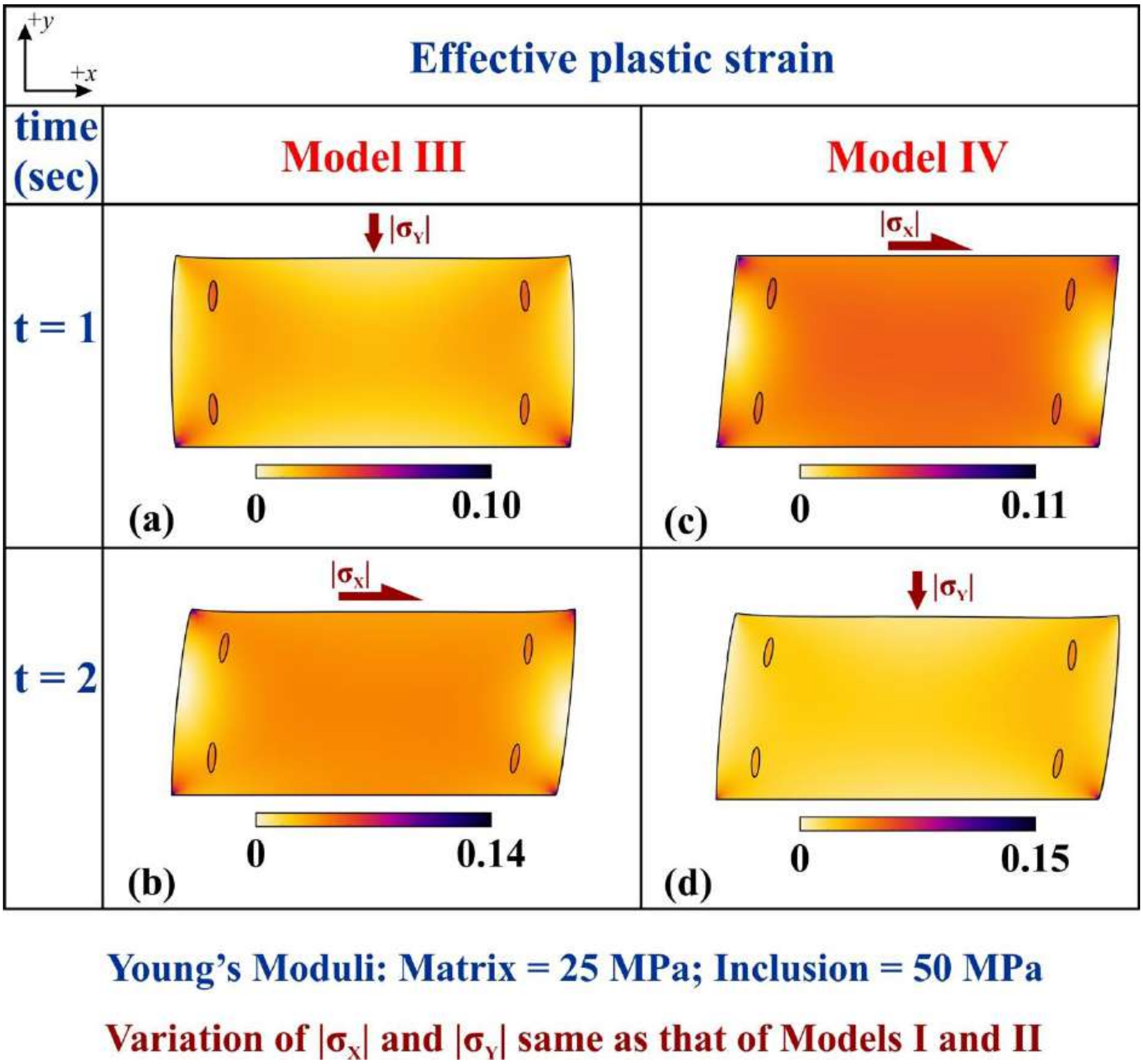

Fig. S9. Effective plastic strain at the end of each deformation at (t = 1 and 2 sec) for (a,b) Model III and (c,d) Model IV. The boundary conditions and applied stress conditions for these models are identical to that of Models I and II. The Young's Moduli, however, have been varied as shown.

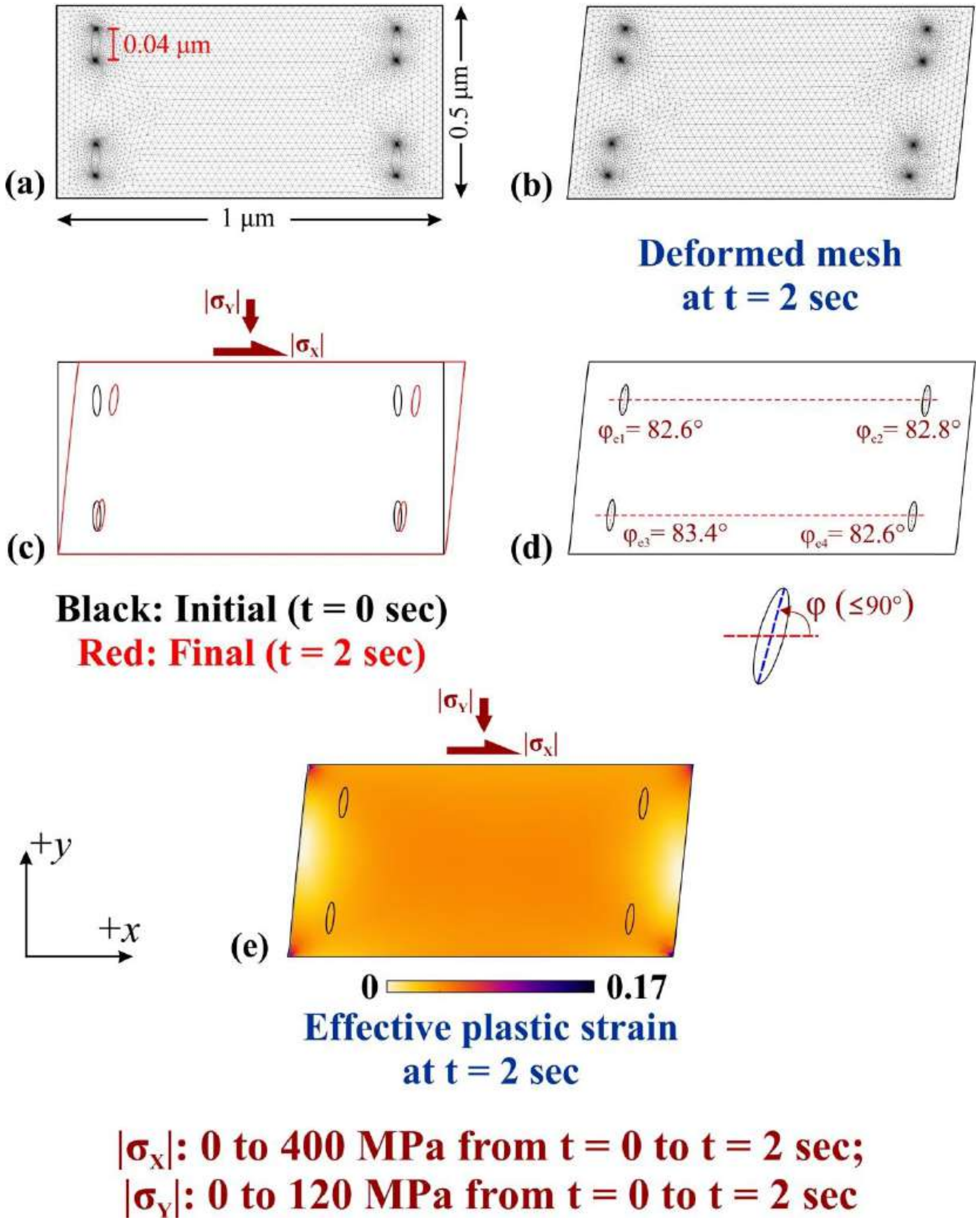

Fig. S10. Results of the general shear deformation simulated using COMSOL Multiphysics v5.4 (first referred at Section A.4 in the Appendix). **(a)** Pre-deformation model setup. **(b)** The deformed mesh. **(c)** Initial and final geometries of the rectangular and elliptical domains. **(d)** Acute angles (measured counter-clockwise) between the long axes (blue dotted line) of the ellipses and the shear plane (red dotted lines). **(e)** Variation of the effective plastic strain over the domain at the end of deformation.

Additional References

Aerden, D. G. A. M., Bell, T. H., Puga, E., Sayab, M., Lozano, J. A., de Federico, A. D., 2013. Multi-stage mountain building vs. relative plate motions in the Betic Cordillera deduced from integrated microstructural and petrological analysis of porphyroblast inclusion trails. Tectonophysics 587, 188-206.

Alder, S., Smith, S. A. F., Scott, J. M., 2016. Fault-zone structure and weakening processes in basin-scale reverse faults: The Moonlight Fault Zone, South Island, New Zealand. J. Struct. Geol. 91, 177-194.

Amato, J. M., Johnson, C. M., Baumgartner, L. P., Beard, B. L., 1999. Rapid exhumation of the Zermatt-Saas ophiolite deduced from high-precision Sm-Nd and Rb-Sr geochronology. Earth Planet. Sci. Lett. 171, 425-438.

Ames, L., Tilton, G. R., Zhou, G., 1993. Timing of collision of the Sino-Korean and Yangtse cratons: U-Pb zircon dating of coesite-bearing eclogites. Geology 21, 339-342.

Augier, R., Jolivet, L., Robin, C., 2005. Late Orogenic doming in the eastern Betic Cordilleras: Final exhumation of the Nevado-Filabride complex and its relation to basin genesis. Tectonics, 24. doi: 10.1029/2004TC001687

Barka, A., 1992. The North Anatolian fault zone. Ann. Tectontcae, Suppl. 6, 164-195.

Barnes, S. J., Couture, J. F., Sawyer, E. W., Bouchaib, C., 1993. Nickel-copper occurrences in the Belleterre-Angliers Belt of the Pontiac Subprovince and the use of Cu-Pd ratios in interpreting platinum-group element distributions. Econ. Geol. 88, 1402-1418.

Baxter, A. T., Aitchison, J. C., Zyabrev, S. V., 2009. Radiolarian age constraints on Mesotethyan ocean evolution, and their implications for development of the Bangong–Nujiang suture, Tibet. J. Geol. Soc. 166, 689-694.

Beaumont, C., Jamieson, R. A., 2010. Himalayan–Tibetan Orogeny: channel flow versus (critical) wedge models, a false dichotomy? In: Leech, M. L., Klemperer, S. L., Mooney, W. D. (Eds.), Proceedings for the 25th Himalaya-Karakoram-Tibet Workshop, U.S. Geol. Surv. Open-File Report.

Beidinger, A., Decker, K., 2016. Paleogene and Neogene kinematics of the Alpine-Carpathian fold-thrust belt at the Alpine-Carpathian transition. Tectonophys. 690, 263-287.

Bell, T. H., Johnson, S. E., 1989b. The role of deformation partitioning in the deformation and recrystallization of plagioclase and K-feldspar in the Woodroffe Thrust mylonite zone, central Australia. J. Metamorph. Geol. 7, 151-168.

Borradaile, G. J., 2001. Paleomagnetic vectors and tilted dikes. Tectonophysics 333, 417-426.

Bielski, M., 1982. Stages in the Arabian-Nuvian Massif in Sinai (unpublished Ph.D. Thesis) – Hebrew University, Jerusalem, 155 pp

Briggs, S. M., Yin, A., Manning, C. E., Chen, Z. L., Wang, X. F., Grove, M., 2007. Late Paleozoic tectonic history of the Ertix Fault in the Chinese Altai and its implications for the development of the Central Asian Orogenic System. Geol. Soc. Am. Bull. 119, 944-960.

Butler, R. W., Tavarnelli, E., Grasso, M., 2006. Structural inheritance in mountain belts: an Alpine–Apennine perspective. J. Struct. Geol. 28, 1893-1908.

Butler, R. W. H., Wheeler, J., Treloar, P. J., Jones, C., 2000. Geological structure of the southern part of the Nanga Parbat massif, Pakistan Himalaya, and its tectonic implications.In: Khan M A, Treloar, P. J., Searle, M. P., Jan, M. Q. (Eds.), Tectonics of theNanga Parbat Syntaxis and the Western Himalaya. Geological Societyof London Special Publications. 170, 123-136.

Calabro, M. D., Schmidt, D. A., Roering, J. J., 2010. An examination of seasonal deformation at the Portuguese Bend landslide, southern California, using radar interferometry. J. Geophys. Res.: Earth Surface, 115. doi: 10.1029/2009JF001314

Carmignani, L., Kligfield, R., 1990. Crustal extension in the Northern Apennines: the transition from compression to extension in the Alpi Apuane core complex. Tectonics 9, 1275-1303.

Carminati, E., Doglioni, C., 2012. Alps vs. Apennines: the paradigm of a tectonically asymmetric Earth. Earth-Sci. Rev. 112, 67-96.

Carosi, R., Montomoli, C., Iaccarino, S., 2018. 20 years of geological mapping of the metamorphic core across Central and Eastern Himalayas. Earth-Sci. Rev. 177, 124-138.

Ceccato, A., Pennacchioni, G., 2018. Structural evolution of the Rieserferner pluton in the framework of the Oligo-Miocene tectonics of the Eastern Alps. J. Struct. Geol. 116, 64-80.

Chattopadhyay, A., Khasdeo, L., 2011. Structural evolution of Gavilgarh-Tan Shear Zone, central India: A possible case of partitioned transpression during Mesoproterozoic oblique collision within Central Indian Tectonic Zone. Precambr. Res. 186, 70-88.

Chârusiri, P., Clark, A. H., Farrar, E., Archibald, D., Chârusiri, B., 1993. Granite belts in Thailand: evidence from the 40Ar/39Ar geochronological and geological syntheses. J. Southeast Asian Earth Sci. 8, 127-136.

Chauvet, A., Dallmeyer, R. D., 1992. 40Ar/39Ar mineral dates related to Devonian extension in the southwestern Scandinavian Caledonides. Tectonophys. 210, 155-177.

Chemale Jr, F., Mallmann, G., de Fátima Bitencourt, M., Kawashita, K., 2012. Time constraints on magmatism along the Major Gercino Shear Zone, southern Brazil: implications for West Gondwana reconstruction. Gond. Res. 22, 184-199.

Chough, S. K., Kwon, S. T., Ree, J. H., Choi, D. K., 2000. Tectonic and sedimentary evolution of the Korean peninsula: a review andnew view. Earth-Sci. Rev. 52, 175–235

Colgan, J. P., Howard, K. A., Fleck, R. J., Wooden, J. L., 2010. Rapid middle Miocene extension and unroofing of the southern Ruby Mountains, Nevada. Tectonics 29, TC 6022.doi: 10.1029/2009TC002655

Collettini, C., Di Stefano, G., Carpenter, B., Scarlato, P., Tesei, T., Mollo, S., Trippetta, F., Marone, C., Romeo, G., Chiaraluce, L., 2014. A novel and versatile apparatus for brittle rock deformation. Int. J. Rock Mech. Min. Sci. 66, 114-123.

Darby, B. J., Ritts, B. D., 2007. Mesozoic structural architecture of the Lang Shan, North-Central China: intraplate contraction, extension, and synorogenic sedimentation. J. Struct. Geol. 29, 2006-2016.

Debenham, N., King, R. C., Holford, S. P., 2018. The influence of a reverse-reactivated normal fault on natural fracture geometries and relative chronologies at Castle Cove, Otway Basin. J. Struct. Geol. 112, 112-130.

Decarlis, A., Dallagiovanna, G., Lualdi, A., Maino, M., Seno, S., 2013. Stratigraphic evolution in the Ligurian Alps between Variscan heritages and the Alpine Tethys opening: A review. Earth-Sci. Rev. 125, 43-68.

de Sigoyer, J., Guillot, S., Dick, P., 2004. Exhumation of the ultrahigh-pressure Tso Morari unit in eastern Ladakh (NW Himalaya): A case study. Tectonics 23.doi: 10.1029/2002TC001492

Dezes, P. J., Vannay, J. C., Steck, A., Bussy, F., Cosca, M., 1999. Synorogenic extension: Quantitative constraints on the age and displacement of the Zanskar shear zone (northwest Himalaya). Geol. Soc. Am. Bull. 111, 364-374.

Dias, R., Ribeiro, A., 1995. The Ibero-Armorican Arc: A collision effect against an irregular continent?. Tectonophysics 246, 113-128.

Doglioni, C., Carminati, E., Cuffaro, M., Scrocca, D., 2007. Subduction kinematics and dynamic constraints. Earth-Sci. Rev. 83, 125-175.

Dusel–Bacon, C., Hansen, V. L., Scala, J. A., 1995. High-pressure amphibolite facies dynamic metamorphism and the Mesozoic tectonic evolution of an ancient continental margin, east-central Alaska. J. Metamorph. Geol. 13, 9-24.

Epard, J. L., & Steck, A., 2008. Structural development of the Tso Morari ultra-high pressure nappe of the Ladakh Himalaya. Tectonophysics 451, 242-264.

Dilek, Y., Thy, P., Moores, E. M., and Ramsden, T. W., 1990. Tectonic evolution of the Troodos ophiolite within the Tethyan framework. Tectonics9, 811–823.

Fernández, R. D., Arenas, R., Pereira, M. F., Sánchez-Martínez, S., Albert, R., Parra, L. M. M., Pascual, F. J. R., Matas, J., 2016. Tectonic evolution of Variscan Iberia: Gondwana–Laurussia collision revisited. Earth Sci.Rev. 162, 269-292.

Finch, M., Hasalová, P., Weinberg, R. F., Fanning, C. M., 2014. Switch from thrusting to normal shearing in the Zanskar shear zone, NW Himalaya: Implications for channel flow. GSA Bull. 126, 892-924.

Fowler A, Hassen I. S., Osman A. F., 2010. Neoproterozoic structural evolution of SE Sinai, Egypt: I. Re-investigation of the structures and deformation kinematics of the Um Zariq and Malhaq Formations, northern Wadi Kid area. J. Afr. Earth Sci. 58, 507–525.

Gapais, D., Pêcher, A., Gilbert, E., Ballèvre, M., 1992. Synconvergence spreading of the higher Himalaya crystalline in Ladakh. Tectonics 11, 1045-1056.

Gehrels, G. E., DeCelles, P. G., Martin, A., Ojha, T. P., Pinhassi, G., Upreti, B. N., 2003. Initiation of the Himalayan orogen as an early Paleozoic thin-skinned thrust belt. GSA Today 13, 4-9.

Ghosh, J. G., de Wit, M. J., Zartman, R. E., 2004. Age and tectonic evolution of Neoproterozoic ductile shear zones in the Southern Granulite Terrain of India, with implications for Gondwana studies. Tectonics, 23. doi: 10.1029/ 2002TC001444.

Gilley, L. D., Harrison, T. M., Leloup, P. H., Ryerson, F. J., Lovera, O. M., & Wang, J. H., 2003. Direct dating of left-lateral deformation along the Red River shear zone, China and Vietnam. J. Geophys. Res.: Solid Earth, 108.doi: 10.1029/2001JB001726

Grand, T., Lapierre, H., Mascle, G. H., Ohnenstetter, M., Angelier, J.,1993. Superimposed tectonics of the Cyprus ophiolitic massifs. Tectonics. 12, 93–101.

Grønlie, A., Roberts, D., 1989. Resurgent strike-slip duplex development along the Hitra-Snåsa and Verran faults, Møre-Trøndelag fault zone, central Norway. J. Struct. Geol. 11, 295-305.

Guillot, S., 1999. An overview of the metamorphic evolution in central Nepal. J. Asian Earth Sci. 17, 713-725.

Guillot, S., de Sigoyer, J., Lardeaux, J. M., Mascle, G., 1997. Eclogitic metasediments from the Tso Morari area (Ladakh, Himalaya): Evidence for continental subduction during India-Asia convergence. Contrib. Min. Petrol. 128, 197-212.

Han, Y., Zhao, G., 2018. Final amalgamation of the Tianshan and Junggar orogenic collage in the southwestern Central Asian Orogenic Belt: Constraints on the closure of the Paleo-Asian Ocean. Earth-Sci.Rev. 186, 129-152.

Hancock, P. L., Barka, A. A., 1980. Plio-Pleistocene reversal of displacement on the North Anatolian fault zone. Nature 286, 591.

Hansen, V. L., 1989. Structural and kinematic evolution of the Teslin suture zone, Yukon: record of an ancient transpressional margin. J. Struct. Geol. 11, 717-733.

Hansen, V. L., Dusel-Bacon, C., 1998. Structural and kinematic evolution of the Yukon-Tanana upland tectonites, east-central Alaska: A record of late Paleozoic to Mesozoic crustal assembly. Geol. Soc. Am. Bull. 110, 211-230.

Harris, N. B. W., Santosh, M., Taylor, P. N., 1994. Crustal evolution in South India: constraints from Nd isotopes. J. Geol. 102, 139-150.

Hazarika, D., Paul, A., Wadhawan, M., Kumar, N., Sen, K., Pant, C. C., 2017. Seismotectonics of the Trans-Himalaya, Eastern Ladakh, India: Constraints from moment tensor solutions of local earthquake data. Tectonophysics 698, 38-46.

He, Z. Y., Klemd, R., Yan, L. L., Zhang, Z. M., 2018.The origin and crustal evolution of microcontinents in the Beishan orogen of the southern Central Asian Orogenic Belt. Earth-Sci. Rev. 185, 1-14

Heidbach, O., Rajabi, M., Cui, X., Fuchs, K., Müller, B., Reinecker, J., Reiter, K., Tingay, M., Wenzel, F., Xie, F., Ziegler, M. O., Zoback, M., 2018. The World Stress Map database release 2016: Crustal stress pattern across scales. Tectonophysics 744, 484-498.

Holdsworth, R. E., Pinheiro, R. V., 2000. The anatomy of shallow-crustal transpressional structures: insights from the Archaean Carajás fault zone, Amazon, Brazil. J. Struct. Geol. 22, 1105-1123.

Holloway, S., Chadwick, R. A., 1986. The Sticklepath-Lustleigh fault zone: Tertiary sinistral reactivation of a Variscan dextral strike-slip fault. J. Geol. Soc. 143, 447-452.

Holm, R. J., Rosenbaum, G., Richards, S. W., 2016. Post 8 Ma reconstruction of Papua New Guinea and Solomon Islands: Microplate tectonics in a convergent plate boundary setting. Earth-Sci. Rev. 156, 66-81.

Hubert-Ferrari, A., King, G., van der Woerd, J., Villa, I., Altunel, E., Armijo, R., 2009. Long-term evolution of the North Anatolian Fault: new constraints from its eastern termination. In: Van Hinsbergen, D. J. J., Edwards, M. A., Govers, R. (Eds.), Collision and Collapse at the Africa-Arabia-Eurasia Subduction Zone. Geological Society of London Special Publications 311, 133-154.

Javadi, H. R., Ghassemi, M. R., Shahpasandzadeh, M., Guest, B., Ashtiani, M. E., Yassaghi, A. L. I., Kouhpeyma, M., 2013. History of faulting on the Doruneh Fault System: implications for the kinematic changes of the Central Iranian Microplate. Geol. Mag. 150, 651-672.

Joshi, M., 1999. Evolution of the basal shear zone of the Almora Nappe, Kumaun Himalaya. In: Jain, A. K., Manickavasagam, R. M. (Eds.), Geodynamics of the Himalaya. Gond. Res. Gr. Mem. 6, 69-80.

Joyce, N. L., Ryan, J. J., Colpron, M., Hart, C. J. R., Murphy, D. C., 2015. A compilation of 40Ar/39Ar age determinations for igneous and metamorphic rocks, and mineral occurrences from central and southeast Yukon. Geol. Surv. Can.Open File 7924, 297446.

Jiawei, X., Guang, Z., 1994. Tectonic models of the Tan-Lu fault zone, eastern China. Int. Geol. Rev. 36, 771-784.

Kayen, R. E., Lee, H. J., Hein, J. R., 2002. Influence of the Portuguese Bend landslide on the character of the effluent-affected sediment deposit, Palos Verdes margin, southern California. Cont. Shelf Res. 22, 911-922.

Keep, M., 1996. The Pinal Schist, southeast Arizona, USA: contraction of a Palaeoproterozoic rift basin. J. Geol. Soc. 153, 979-993.

Lacassin, R., Maluski, H., Leloup, P. H., Tapponnier, P., Hinthong, C., Siribhakdi, K., Chuaviroj, S., Charoenravat, A., 1997. Tertiary diachronic extrusion and deformation of western Indochina: structural and $^{40}Ar/^{39}Ar$ evidence from NW Thailand. J. Geophys. Res.: Solid Earth, 102.doi: 10.1029/96JB03831

Langille, J. M., Jessup, M. J., Cottle, J., Ahmad, T., 2014. Kinematic and thermal studies of the Leo Pargil Dome: Implications for synconvergent extension in the NW Indian Himalaya. Tectonics 33, 1766-1786.

Lee, J., Miller, E. L., Sutter, J. F., 1987. Ductile strain and metamorphism in an extensional tectonic setting: a case study from the northern Snake Range, Nevada, USA. In: Coward, M.P., Dewey, J. F., Hancock, P. L. (Eds.), Continental Extensional Tectonics. Geological Societyof London Special Publications 28, 267-298.

Li, J., Hou, G., 2019. Stress development in heterogeneous lithosphere: insights into earthquake initiation in the Tan-Lu Fault Zone. Tectonophysics

Licciardi, A., Eken, T., Taymaz, T., Agostinetti, N. P., Yolsal-Çevikbilen, S., 2018. Seismic anisotropy in central North Anatolian Fault Zone and its implications on crustal deformation. Phys. Earth Planet. Inter. 277, 99-112.

Lin, A., Maruyama, T., Aaron, S., Michibayashi, K., Camacho, A., Kano, K. I., 2005. Propagation of seismic slip from brittle to ductile crust: Evidence from pseudotachylyte of the Woodroffe thrust, central Australia. Tectonophysics 402, 21-35.

Little, T. A., Hacker, B. R., Gordon, S. M., Baldwin, S. L., Fitzgerald, P. G., Ellis, S., Korchinski, M., 2011. Diapiric exhumation of Earth's youngest (UHP) eclogites in the gneiss domes of the D'Entrecasteaux Islands, Papua New Guinea. Tectonophysics 510, 39-68.

Liu, M., Yang, Y., Stein, S., Klosko, E., 2002. Crustal shortening and extension in the Central Andes: insights from a viscoelastic model. In: Stein, S., Freymuller, G. (Eds.), Plate Boundary Zones, AGU Geodyn. Ser. 30, 325-339.

Llana-Fúnez, S., Marcos, A., 2007. Convergence in a thermally softened thick crust: Variscan intracontinental tectonics in Iberian plate rocks. Terra Nova 19, 393-400.

Llana-Fúnez, S., Marcos, A., 2001. The Malpica–Lamego Line: a major crustal-scale shear zone in the Variscan belt of Iberia. J. Struct. Geol. 23, 1015-1030.

Löw, S., 1987. Die tektono-metamorphe Entwicklung der Nördlichen Adula-Decke. Beiträge zur Geologischen Karte der Schweiz N.F., 161, 1–84.

Machado, N., Lindenmayer, Z., Krogh, T. E., Lindenmayer, D., 1991. U-Pb geochronology of Archean magmatism and basement reactivation in the Carajás area, Amazon shield, Brazil. Precambr. Res. 49, 329-354.

MacLeod, C. J., Murton, B. J., 1993. Structure and tectonic evolution of the Southern Troodos transform fault zone, Cyprus. In: Prichard, H. M., Alabaster, T., Harris, N. B. W., Neary, C. R. (Eds.), Magmatic Processes and Plate Tectonic. Geological Societyof London Special Publications 76, 141-176.

Mancktelow, N.S., Stöckli, D., Grollimund, B., Müller, W., Fügenschuh, B., Viola, G., Seward, D. & Villa, I., 2001. TheDAV and Periadriatic fault systems in the eastern Alps southof the Tauern Window. Int. J. Earth Sci. 90, 593–622.

Matte, P., 2001. The Variscan collage and orogeny (480–290 Ma) and the tectonic definition of the Armorica microplate: a review. Terra Nova 13, 122-128.

Meng, Q. R., Wu, G. L., Fan, L. G., Wei, H. H., 2019. Tectonic evolution of early Mesozoic sedimentary basins in the North China block. Earth-Sci. Rev. 190, 416-438

Michibayashi, K., Gerbert-Gaillard, L., Nicolas, A., 2000. Shear sense inversion in the Hilti mantle section (Oman ophiolite) and active mantle uprise. Marine Geophys. Res. 21, 259-268.

Moores, E. M., Vine, F. J., 1971. The Troodos Massif, Cyprus and other ophiolites as oceanic crust: evaluation and implications. Phil. Trans. R. Soc. Lond. A268, 443-467.

Najman, Y., Jenks, D., Godin, L., Boudagher-Fadel, M., Millar, I., Garzanti, E., Horstwood, M., Bracciali, L., 2017. The Tethyan Himalayan detrital record shows that India–Asia terminal collision occurred by 54 Ma in the Western Himalaya. Earth Planet. Sci. Lett. 459, 301-310.

Neumann, N. L., Gibson, G. M., Southgate, P. N., 2009. New SHRIMP age constraints on the timing and duration of magmatism and sedimentation in the Mary Kathleen Fold Belt, Mt Isa Inlier, Australia. Aust. J. Earth Sci. 56, 965-983.

Ngako, V., Affaton, P., Njonfang, E., 2008. Pan-African tectonics in northwestern Cameroon: implication for the history of western Gondwana. Gond. Res. 14, 509-522.

Norris, R. J., Carter, R. M., Turnbull, I. M., 1978. Cainozoic sedimentation in basins adjacent to a major continental transform boundary in southern New Zealand. J. Geol. Soc. 135, 191-205.

Norris, R. J., Koons, P. O., Cooper, A. F., 1990. The obliquely-convergent plate boundary in the South Island of New Zealand: implications for ancient collision zones. J. Struct. Geol. 12, 715-725.

Northrup, C. J., Royden, L. H., Burchfiel, B. C., 1995. Motion of the Pacific plate relative to Eurasia and its potential relation to Cenozoic extension along the eastern margin of Eurasia. Geology 23, 719-722.

Nugraha, A. D., Ohmi, S., Mori, J., Shibutani, T., 2013. High resolution seismic velocity structure around the Yamasaki fault zone of southwest Japan as revealed from travel-time tomography. Earth Planets Space, 65, 871-881.

Oliver, N.H.S., Rawling, T.J., Cartwright, I. Pearson, P., 1994. High-temperature fluid-rock interaction and scapolitization in an extension-related hydrothermal system, Mary Kathleen, Australia. J. Petrol. 35, 1455-1491

Otofuji, Y. I., Itaya, T., Matsuda, T., 1991. Rapid rotation of southwest Japan—palaeomagnetism and K-Ar ages of Miocene volcanic rocks of southwest Japan. Geophys. J. Int. 105, 397-405.

Palin, R. M., Reuber, G. S., White, R. W., Kaus, B. J., Weller, O. M., 2017. Subduction metamorphism in the Himalayan ultrahigh-pressure Tso Morari massif: An integrated geodynamic and petrological modelling approach. Earth Planet. Sci. Lett. 467, 108-119.

Park, R. G., Crane, A., Niamatullah, M., 1987.Early Proterozoic structure and kinematic evolution of the southern mainland Lewisian. In: Park, R. G., Tarney, J. (Eds.), Evolution of the Lewisian and ComparablePrecambrian High Grade Terrains.Geological Societyof London Special Publications 27, 139-151.

Passarelli, C. R., Basei, M. A., Siga Jr, O., Mc Reath, I., Neto, M. D. C. C., 2010. Deformation and geochronology of syntectonic granitoids emplaced in the Major Gercino Shear Zone, southeastern South America. Gond. Res. 17, 688-703.

Passchier, C. W., 1990. Reconstruction of deformation and flow parameters from deformed vein sets. Tectonophysics 180, 185-199.

Pearson, P. J., Holcombe, R. J. Page, R. W., 1992. Synkinematic emplacement of the Middle Proterozoic Wonga Batholith into a mid-crustal extensional shear zone, Mount Isa Inlier, Queensland, Australia. In: Stewart, A. J., Blake, D. H. (Eds.,) Detailed studies of the Mount Isa Inlier. Aust. Geol. Surv. Org. Bull. 289–328.

Platt, J. P., Argles, T. W., Carter, A., Kelley, S. P., Whitehouse, M. J., Lonergan, L., 2003. Exhumation of the Ronda peridotite and its crustal envelope: constraints from thermal modelling of a P–T–time array. J. Geol. Soc. 160, 655-676.

Platt, J. P., Anczkiewicz, R., Soto, J. I., Kelley, S. P., Thirlwall, M., 2006. Early Miocene continental subduction and rapid exhumation in the western Mediterranean. Geology 34, 981-984.

Platt, J. P., Behr, W. M., Johanesen, K., Williams, J. R., 2013. The Betic-Rif arc and its orogenic hinterland: a review. Ann. Rev. Earth Planet. Sci. 41, 313-357.

Pleuger, J., Mancktelow, N., Zwingmann, H., Manser, M., 2012. K–Ar dating of synkinematic clay gouges from Neoalpine faults of the Central, Western and Eastern Alps. Tectonophysics 550, 1-16.

Puga, E., Díaz de Federico, A., Fanning, M., Nieto, J. M., Rodríguez Martínez-Conde, J. Á., Díaz Puga, M. Á., Lozano, J. A., Bianchini, G., Natali, C., Beccaluva, L., 2017. The Betic ophiolites and the mesozoic evolution of the western Tethys. Geosciences 7, 31.

Putnis, A., Jamtveit, B., Austrheim, H., 2017. Metamorphic processes and seismicity: the Bergen Arcs as a natural laboratory. J. Petrol. 58, 1871-1898.

Raimondo, T., Hand, M., Collins, W. J., 2014. Compressional intracontinental orogens: Ancient and modern perspectives. Earth-Sci. Rev. 130, 128-153.

Rajabi, M., Tingay, M., Heidbach, O., Hillis, R., Reynolds, S., 2017. The Present-day stress field of Australia. Earth-Sci. Rev. 168, 165-189.

Rajesh, H. M., Santosh, M., Yoshida, M., 1996. The felsic magmatic province in East Gondwana: implications for Pan-African tectonics. J. Southeast Asian Earth Sci. 14, 275-291.

Reddy, S. M., Wheeler, J., Butler, R. W. H., Cliff, R. A., Freeman, S., Inger, S., Pickles, C., Kelley, S. P., 2003. Kinematic reworking and exhumation within the convergent Alpine Orogen. Tectonophys. 365, 77-102.

Redfield, T. F., Braathen, A., Gabrielsen, R. H., Osmundsen, P. T., Torsvik, T. H., Andriessen, P. A. M., 2005. Late Mesozoic to early Cenozoic components of vertical separation across the Møre–Trøndelag Fault Complex, Norway. Tectonophysics 395, 233-249.

Redfield, T. F., Torsvik, T. H., Andriessen, P. A. M., Gabrielsen, R. H., 2004. Mesozoic and Cenozoic tectonics of the Møre Trøndelag Fault Complex, central Norway: constraints from new apatite fission track data. Phys. Chem. Earth 29, 673-682.

Robyr, M., Epard, J. L., El Korh, A., 2014. Structural, metamorphic and geochronological relations between the Zanskar Shear Zone and the Miyar Shear Zone (NW Indian Himalaya): Evidence for two distinct tectonic structures and implications for the evolution of the High Himalayan Crystalline of Zanskar. J. Asian Earth Sci. 79, 1-15.

Rosenberg, C. L., Schneider, S., Scharf, A., Bertrand, A., Hammerschmidt, K., Rabaute, A., Brun, J. P., 2018. Relating collisional kinematics to exhumation processes in the Eastern Alps. Earth-Sci Rev. 176, 311-344.

Rossetti, F., Glodny, J., Theye, T., Maggi, M., 2015. Pressure–temperature–deformation–time of the ductile Alpine shearing in Corsica: From orogenic construction to collapse. Lithos, 218, 99-116.

Ryan, J.J., Zagorevski, A., Roots, C.F., and Joyce, N., 2014, Paleozoic tectonostratigraphy of the northern StevensonRidge area, Yukon: Geol. Sur. Can. Curr. Res.4. 13 pp.

Sacks, P. E., Nambiar, C. G., Walters, L. J., 1997. Dextral Pan-African shear along the southwestern edge of the Achankovil Shear Belt, South India: constraints on Gondwana reconstructions. J. Geol. 105, 275-284.

Sawyer, E. W., Barnes, S. J., 1994. Thrusting, magmatic intraplating, and metamorphic core complex development in the Archaean Belleterre-Angliers greenstone belt, Superior Province, Quebec, Canada. Precambr. Res. 68, 183-200.

Schulmann, K., Lexa, O., Janoušek, V., Lardeaux, J. M., Edel, J. B., 2014. Anatomy of a diffuse cryptic suture zone: an example from the Bohemian Massif, European Variscides. Geology 42, 275-278.

Searle, M., Corfield, R. I., Stephenson, B. E. N., McCarron, J. O. E., 1997. Structure of the North Indian continental margin in the Ladakh–Zanskar Himalayas: implications for the timing of obduction of the Spontang ophiolite, India–Asia collision and deformation events in the Himalaya. Geol. Mag. 134, 297-316.

Sharma, R. S., 2009. Cratons and Fold Belts of India.Springer, Berlin, Heidelberg. 231-261

Srivastava, P., Mitra, G., 1996. Deformation mechanisms and inverted thermal profile in the North Almora Thrust mylonite zone, Kumaon Lesser Himalaya, India. J. Struct. Geol. 18, 27-39.

Stacey, A., Totterdell, J., Heike, I. S., Mitchell, C., 2013. Geology and Hydrocarbon Prospectivity of the Deepwater Otway and Sorell Basins, Offshore Southeastern Australia Geosci. Aust. Canberra Record 2013/02.

Stern, R. J., Li, S. M., Keller, G. R., 2018. Continental crust of China: A brief guide for the perplexed. Earth-Sci. Rev. 179, 72-94.

Tapponnier, P., Peltzer, G., Armijo, R., 1986. On the mechanics of the collision between India and Asia.In: Coward, M. P., Ries, A. C. (Eds.), Collision Tectonics. Geological Societyof London Special Publications 19, 113-157.

Tempelman-Kluit, D. J., 1979, Transported cataclasite, ophiolite and granodiorite in Yukon: Evidence of arc-continentcollision: Geol. Surv.Can. Pap. 79–14,27 pp.

Torsvik, T. H., Smethurst, M. A., Meert, J. G., Van der Voo, R., McKerrow, W. S., Brasier, M. D., Sturt, B. A., Walderhaug, H. J., 1996. Continental break-up and collision in the Neoproterozoic and Palaeozoic—a tale of Baltica and Laurentia. Earth-Sci. Rev. 40, 229-258.

Torvela, T., Mänttäri, I., Hermansson, T., 2008.Timing of deformation phases within the South Finland shear zone, SW Finland.Precambr. Res. 160, 277-298.

Toteu, S. F., Penaye, J., Djomani, Y. P., 2004. Geodynamic evolution of the Pan-African belt in central Africa with special reference to Cameroon. Can. J. Earth Sci. 41, 73-85.

Toteu, S. F., Van Schmus, W. R., Penaye, J., Michard, A., 2001. New U–Pb and Sm–Nd data from north-central Cameroon and its bearing on the pre-Pan African history of central Africa. Precambr. Res. 108, 45-73.

Tucker, R. D., Krogh, T. E., 1988. Geochronological investigation of the Ingdal granite gneiss and discordant pegmatites from the Western Gneiss region, Norway. Norsk Geologisk Tidsskrift, 68, 201-210.

Turco, E., Macchiavelli, C., Mazzoli, S., Schettino, A., Pierantoni, P. P., 2012.Kinematic evolution of Alpine Corsica in the framework of Mediterranean mountain belts. Tectonophysics 579, 193-206.

Turnbull, I. M., Barry, J. M., Carter, R. M., Norris, R. J., 1975. The Bobs Cove beds and their relationship to the Moonlight Fault Zone. J. Royal Soc. New Zealand 5, 355-394.

van der Wal, D., Vissers, R. L., 1996. Structural petrology of the Ronda peridotite, SW Spain: deformation history. J. Petrol. 37, 23-43.

Walker, R. T., Fattahi, M., 2011. A framework of Holocene and Late Pleistocene environmental change in eastern Iran inferred from the dating of periods of alluvial fan abandonment, river terracing, and lake deposition. Quat. Sci. Rev. 30, 1256-1271.

Walpersdorf, A., Manighetti, I., Mousavi, Z., Tavakoli, F., Vergnolle, M., Jadidi, A., Hatzfeld, D., Aghamohammadi, A., Bigot, A., Djamour , Y., Nankali , H., Sedighi, M., 2014. Present-day kinematics and fault slip rates in eastern Iran, derived from 11 years of GPS data, J. Geophys. Res. Solid Earth, 119, 1359–1383.

Wang, Y., Zhou, L., Liu, S., Li, J., Yang, T., 2018. Post-cratonization deformation processes and tectonic evolution of the North China Craton. Earth-Sci. Rev. 177, 320-365.

Watanabe, K., Nishigami, K., Nakao, S., Matsumura, K., 1996. Crustal activity of the Yamasaki fault zone before andafter the 1995 Hyogo-ken Nanbu earthquake, Annu. Disas. Prev. Res. Ints., Kyoto Univ., 39B-1, (in Japanese with English abstract)

Weijermars, R., 1991. Geology and tectonics of the Betic Zone, SE Spain. Earth-Sci. Rev. 31, 153-236.

Wex, S., Mancktelow, N. S., Hawemann, F., Camacho, A., Pennacchioni, G., 2017. Geometry of a large-scale, low-angle, midcrustal thrust (Woodroffe Thrust, central Australia). Tectonics 36, 2447-2476.

Wex, S., Mancktelow, N., Hawemann, F., Camacho, A., Pennacchioni, G., 2018. Inverted distribution of ductile deformation in the relatively" dry" middle crust across the Woodroffe Thrust, central Australia. Solid Earth 9, 859-878.

Wheeler, J., Park, R. G., Rollinson, H. R., Beach, A., 2010. The Lewisian Complex: insights into deep crustal evolution. In: Law, R. D., Butler, R. W. H., Holdsworth, R. E., Krabbendam, M., Strachan, R. A. (Eds.), Continental Tectonics and Mountain Building: The Legacy of Peach and Horne. Geological Society of London Special Publications 335, 51-79.

Wilhem, C., Windley, B. F., Stampfli, G. M., 2012. The Altaids of Central Asia: a tectonic and evolutionary innovative review. Earth-Sci. Rev. 113, 303-341.

Xiao, W., Huang, B., Han, C., Sun, S., Li, J., 2010. A review of the western part of the Altaids: a key to understanding the architecture of accretionary orogens. Gond. Res. 18, 253-273.

Yamamoto, T., 1991. Late Cenozoic dike swarms and tectonic stress field in Japan. Bull. Geol. Surv. Jpn. 42, 131– 148 (in Japanese with English abstract)

Yin, A., Nie, S., 1993. An indentation model for the North and South China collision and the development of the Tan-Lu and Honam fault systems, eastern Asia. Tectonics 12, 801-813.

Zhao, S., Li, S., Li, X., Somerville, I., Cao, H., Liu, X., Wang, P., 2017. Structural analysis of ductile shear zones in the North Qinling Orogen and its implications for the evolution of the Proto-Tethys Ocean. Geol. J. 52, 202-214.